

1 **Spring tropical cyclones modulate near-surface isotopic compositions of**
2 **atmospheric water vapour at Kathmandu, Nepal**

3 Niranjan Adhikari^{1, 2}, Jing Gao^{1, 3, *}, Aibin Zhao¹, Tianli Xu^{1, 4} Manli Chen^{1, 3},
4 Xiaowei Niu¹, Tandong Yao^{1, 3}

5 ¹ *State Key Laboratory of Tibetan Plateau Earth System, Resources and Environment, Institute*
6 *of Tibetan Plateau Research, Chinese Academy of Sciences, Beijing 100101, China*

7 ² *University of Chinese Academy of Sciences, Beijing 100049, China*

8 ³ *Lanzhou University, Lanzhou 733000, China*

9 ⁴ *Kathmandu Centre for Research and Education, Chinese Academy of Sciences –Tribhuvan*
10 *University, Kirtipur 44613, Kathmandu, Nepal*

11 * Correspondence to: Jing Gao, E-mail: gaojing@itpcas.ac.cn

12
13 **Abstract**

14 While westerlies are recognized as a significant moisture transport in Nepal during the
15 pre-monsoon season, precipitation is also attributed to moisture from cyclones originating in the
16 Bay of Bengal (BoB) or the Arabian Sea (AS). Tropical cyclones exhibit negative isotopic values
17 in both precipitation and atmospheric water vapour; however, the factors influencing isotopic
18 fractionation during tropical cyclones remain poorly understood. We present the results of
19 continuous measurements of the isotopic composition of atmospheric water vapour ($\delta^{18}\text{O}_v$, δD_v ,
20 and d-excess_v) at Kathmandu from 7 May to 7 June 2021 during two pre-monsoon cyclones;
21 cyclone Tauktae formed over the Arabian Sea, and cyclone Yaas formed over the Bay of Bengal.
22 Our study reveals that tropical cyclones originating from the BoB and the AS during the pre-

23 monsoon season modulate isotopic signals of near-surface atmospheric water vapour in Nepal.
24 Comparing conditions before and after, we observed a significant depletion of $\delta^{18}\text{O}_v$ and δD_v
25 during both cyclones, attributed to changes in moisture sources (local vs. marine). Convective
26 activity plays a pivotal role in the variability of $\delta^{18}\text{O}_v$ and δD_v during both cyclones, confirmed
27 by the spatial variations of outgoing longwave radiation (OLR) and regional precipitation during
28 both cyclones. We also found a significant negative correlation between $\delta^{18}\text{O}_v/\delta\text{D}_v$ and rainfall
29 amount along the trajectories during cyclone Tauktae, probably resulting from integrated
30 upstream processes linked to the earlier Rayleigh distillation of water vapour via rainfall, rather
31 than local rainfall. The decrease in $\delta^{18}\text{O}_v/\delta\text{D}_v$ during cyclone Yaas is associated with the
32 intensified convection and moisture convergence at the measurement site, while the lower cloud
33 top temperatures (CTT) and lower cloud top pressure (CTP) during intense convection contribute
34 to higher d-excess values at the final stage of cyclone Yaas. This characteristic is missing during
35 cyclone Tauktae. Our results shed light on key processes governing the isotopic composition of
36 atmospheric water vapour at Kathmandu with implications for the monsoon moisture transport
37 and paleoclimate reconstructions of tropical cyclone activity.

38 Keywords: Cyclones; Isotopic composition of atmospheric water vapour; Convection; Moisture
39 convergence; Kathmandu

40

41

42

43 **1 Introduction**

44 Although the Indian summer monsoon accounts for more than 80 % of annual rainfall in
45 Nepal, agricultural activities also rely on precipitation in the pre-monsoon season. Pre-
46 monsoonal rainfall in Nepal is often associated with cyclonic events that provide precipitation to
47 support the timely planting of monsoonal crops. Previous studies have suggested that extreme
48 precipitation in Nepal is mostly fuelled by moisture from the Arabian Sea (AS) and the Bay of
49 Bengal (BoB) (Bohlinger et al., 2017; Boschi and Lucarini, 2019). Higher sea surface
50 temperatures and the westward movement of tropical cyclones formed over the Western Pacific
51 result in cyclones being formed over the BoB and the AS (Mohapatra et al., 2016). The number
52 of cyclones in the AS has increased recently compared to the number of cyclones in the BoB
53 (Pandya et al., 2021). According to the International Best Track Archive for Climate Stewardship
54 (IBTrACS) project (Knapp et al., 2010), in 2019 three cyclones originated in the BoB and five
55 cyclones originated in the AS, due to a rise in sea surface temperature lengthening the cyclone
56 decay period (Li and Chakraborty, 2020). Usually, the impact of cyclones formed over the AS is
57 restricted to the nearest coastal regions. However, in recent years this appears to have changed as
58 cyclones are forming back-to-back over the AS and affecting the entire Indian subcontinent
59 including surrounding regions (Li and Chakraborty, 2020). Cyclone Tauktae affected the
60 livelihoods of people both near the coast and further inland during the pre-monsoon season of
61 2021 (Pandya et al., 2021). The impacts of cyclone Yaas after cyclone Tauktae were also felt in
62 Nepal, where it triggered flooding and landslides in several parts of the country
63 (<https://floodlist.com/asia/nepal-flood-landslide-may-2021/>). As both cyclones hit in short
64 succession, this led to severe agricultural damage in several parts of India at a critical time when
65 farmers were preparing to sow their rice paddies ahead of the monsoon season

66 (<https://reliefweb.int/organization/acaps>). In Nepal, the damage due to Yaas was mostly limited
67 to the Terai regions which experienced intense and continuous rainfall
68 (<https://kathmandupost.com/>). Moisture flux associated with cyclones generally extends over a
69 large area and causes moderate to heavy precipitation along the cyclone path and on the nearest
70 land mass (Chan et al., 2022; Rajeev and Mishra, 2022). It is therefore essential to understand the
71 moisture transport processes of these extreme rainfall events on atmospheric water vapour.

72 With climate change, the amount of water vapour in the atmosphere is also expected to
73 increase, creating scientific interest in the impact of atmospheric water vapour on changing
74 moisture patterns (Hoffmann et al., 2005). The isotopic composition of atmospheric water
75 vapour ($\delta^{18}\text{O}_v$, δD_v , and $d\text{-excess}_v$) contains comprehensive information about the history of
76 moisture exchange (Noone, 2012; Payne et al., 2007; Risi et al., 2008; Worden et al., 2007).
77 Several studies have shown that the isotopic composition is an effective indicator of cyclone
78 activity (Munksgaard et al., 2015; Sun et al., 2022) including cyclone evolution and structure
79 (Lawrence et al., 2002). The atmospheric water vapour and precipitation associated with tropical
80 cyclones tend to have extremely depleted isotopic compositions compared to monsoonal rain
81 (Chen et al., 2021; Jackisch et al., 2022; Munksgaard et al., 2015; Sánchez-Murillo et al., 2019),
82 which may be due to the high condensation efficiency and substantial fractionation associated
83 with cyclones. A few studies found a systematic depletion of heavy isotopes towards the cyclone
84 eye (Lawrence et al., 2002, 1998; Lawrence and Gedzelman, 1996; Sun et al., 2022; Xu et al.,
85 2019). For example, during cyclone Shanshan, Fudeyasu (2008) observed that isotopic depletion
86 in precipitation and water vapour increased radially inward in the cyclone's outer region, likely
87 due to a rainout effect. A study conducted in north-eastern Australia during cyclone Ita in April
88 2014 underlined the role of synoptic-scale meteorological settings in determining the isotopic

89 variability of atmospheric water vapour (Munksgaard et al., 2015). In Fuzhou, China, Xu et al.,
90 (2019) reported a significant depletion in typhoon rain $\delta^{18}\text{O}$ related to the combined effect of
91 large-scale convection, high condensation efficiency, and recycling of isotopically depleted
92 vapour in the rain shield area. Sánchez-Murillo et al., (2019) highlighted the role of convective
93 and stratiform activity as well as precipitation type and amount. The impact of high stratiform
94 fractions and deep convection on isotopic depletion in precipitation during typhoon Lekima was
95 confirmed by Han et al., (2021).

96 Although several studies have examined the isotopic variation of event-based
97 precipitation in Nepal (Acharya et al., 2020; Adhikari et al., 2020; Chhetri et al., 2014), there
98 remains a knowledge gap regarding the isotopic response of atmospheric water vapour during
99 cyclone events. We present for the first time the evolution of the isotopic composition of
100 atmospheric water vapour ($\delta^{18}\text{O}_v$, δD_v , and d-excess) in Kathmandu during two pre-monsoon
101 cyclone events. Isotopic data were collected in 2021, from one week before to one week after the
102 cyclones. A substantial influence of these cyclone events on the sampling site for several days
103 was apparent in the isotopic composition of atmospheric water vapour, showcasing a marked
104 depletion in comparison to normal days. This allowed us to scrutinize fluctuations in isotopic
105 composition with a high temporal resolution and to investigate the atmospheric processes
106 associated with cyclone events that lead to significant depletion in isotopic composition at
107 diurnal scales.

108 **2 Data and methods**

109 **2.1 Site description**

110 The Kathmandu station lies on the southern slope of the Himalayas ($27^{\circ}42' \text{ N}$, $85^{\circ}20' \text{ E}$)
111 at an altitude of approximately 1400 m above sea level. Based on an 18-year-long record from

112 the Department of Hydrology and Meteorology, Government of Nepal (2001 to 2018), this
113 region has an average annual temperature of 19° C and average annual precipitation amount of
114 about 1500 mm, with ~78% of the annual rainfall occurring in the monsoon season from June to
115 September (Adhikari et al., 2020). About 16 % of annual rainfall in Kathmandu occurs in the
116 pre-monsoon season (March to May) with air temperature ranging from 13 to 28° C and an
117 average relative humidity (RH) of 67 %. Advection of the southern branch of westerlies and
118 evaporation from nearby water bodies are the main contributors to pre-monsoonal precipitation
119 (Yu et al., 2016; Chhetri et al., 2014). These arid westerlies, resulted in diminished temperature
120 and relative humidity (RH) within the region while a substantial presence of moisture was
121 observed over extensive areas encompassing the BoB, the AS, India, and surrounding regions
122 including our sampling site during our study period. Figure S1 shows the elevated specific
123 humidity levels at 850 hPa from May 7 to June 7, 2021.

124

125 **2.2 The evolution of cyclones Tauktae and Yaas and weather conditions at** 126 **Kathmandu**

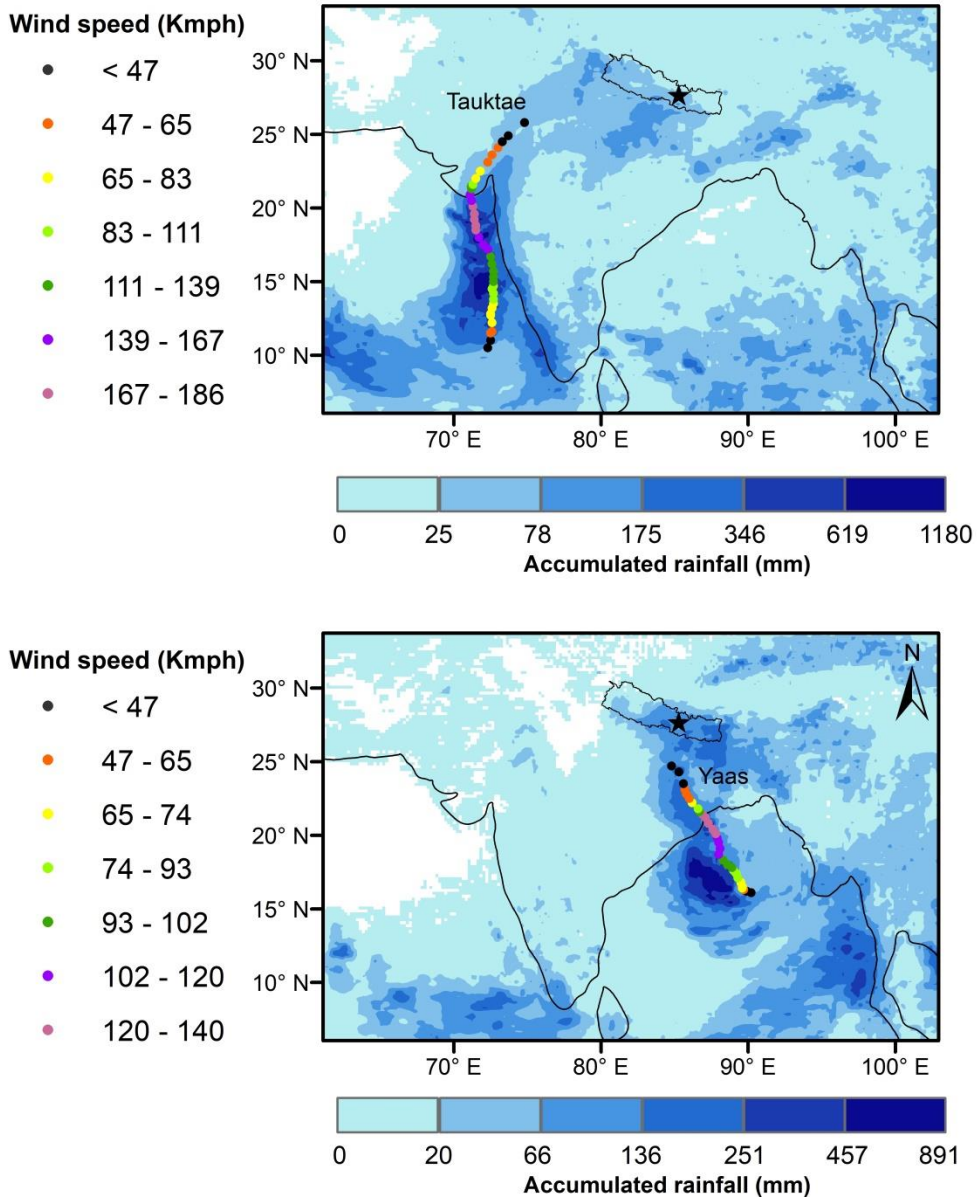
127 Cyclone Tauktae developed as a tropical disturbance on 13 May 2021 over the AS,
128 evolved into a deep depression by 14 May, moved north, and gradually intensified before turning
129 into a cyclonic storm with wind speeds reaching 75 km/h on that same day (Pandya et al., 2021).
130 After making landfall in the Gir-Somnath district of Gujarat, Tauktae continued to strengthen
131 and was classified as an extremely severe cyclonic storm on 17 May reaching maximum wind
132 speeds of 185 km/h (Verma and Gupta, 2021; Pandya et al., 2021). Tauktae weakened into a low
133 depression on 18 May 2021 at 20:30 h Indian Local Time (ILT) and finally dissipated one day
134 later. Due to its large convective area, it brought heavy rainfall to different regions of India and
135 Nepal.

136 The signal of cyclone Tauktae was first detected at the Kathmandu site on 19 May at
137 approximately 03:00 local time (LT), followed by light drizzle. The recorded air temperature was
138 about 22°C, and the relative humidity (RH) was approximately 72%. Within 16 hours, the RH
139 increased from 72% to 91%, while the temperature dropped from 22°C to around 19°C. The
140 maximum RH and minimum temperature were observed on 21 May around 04:00 h LT, reaching
141 92% and 17°C, respectively.

142 Cyclone Yaas started out as a depression over the BoB on 22 May 2021 at 08:30 h ILT
143 and gradually intensified into a deep depression before turning into a cyclonic storm on 24 May
144 at 05:30 h ILT as it moved northeast (Paul and Chowdhury, 2021). The corresponding wind
145 speed and central pressure were recorded as 65 km/h and 990 hPa, respectively. On 24 May
146 around 23:30 h ILT, it intensified into a severe cyclonic storm with wind speeds ranging from 92
147 to 111 km/h before becoming a very severe cyclonic storm on 25 May at 17:30 h ILT with wind
148 speeds from 120 km/h to 139 km/h. It made landfall north of Odisha on 26 May with maximum
149 sustained wind speeds of 130 km/h to 140 km/h and progressively weakened into a depression on
150 27 May before dissipating over northern India on 28 May.

151 The Kathmandu weather station recorded a total of 59.6 mm of precipitation during
152 cyclone Yaas. Intermittent small patches of rainfall commenced on 25 May at 11:00h LT. The
153 main cyclone event occurred from 26 May at 01:00h LT to 29 May at 01:00h LT. Throughout
154 this period, the ground-level RH fluctuated between 84% and 93%, while surface temperature
155 varied between 18°C and 22°C. Notably, all RH values exceeded 80% from 25 May around
156 22:00 h LT to 29 May at 10:00 h LT.

157 Wind speeds, pressure, and cyclone eye location information (3-hour resolution) were
158 retrieved from the best track data of tropical cyclonic disturbances over the north Indian Ocean
159 (available at <https://rsmcnewdelhi.imd.gov.in/>) monitored by India Meteorological Department
160 (IMD). The latter was used to calculate the spatial distance between the cyclone's eye and our
161 measurement location. Figure 1 illustrates the intensity and cumulative rainfall along the paths of
162 the cyclones. A characteristic of both cyclones is the occurrence of rainout along their
163 trajectories, persisting as they move inland.



164

165 **Figure 1** The intensity and track of cyclone Tauktae (Upper panel) and Yaas (Bottom
 166 panel) along with accumulated rainfall during Tauktae (from 14 to 20 May 2021) and Yaas
 167 (24 to 28 May 2021). The intensity and track of cyclones were retrieved from the best track
 168 data of tropical cyclonic disturbance over the north Indian Ocean monitored by IMD and

169 **rainfall data was retrieved from the Integrated Multi-satellite Retrievals provided by the**
170 **Global Precipitation Measurement program (GPM, IMERG dataset).**

171 **2.3 Isotope measurements**

172 Near-surface $\delta^{18}\text{O}_v$ and δD_v were measured continuously using a Picarro L2130-i
173 analyser based on wavelength-scanned cavity ring-down spectroscopy (WS-CRDS) (Brand et al.,
174 2009), located at the Kathmandu Centre for Research and Education (KCRE), Nepal. The
175 sampling inlet consisting of a heated copper tube mounted 7 m above the ground protected with a
176 plastic hood and a 10 L min^{-1} pump transported the sample from the inlet to the analyser. The
177 automated standard delivery module (SDM) was used for calibration, with each calibration made
178 using two reference standards calibrated against Vienna Standard Mean Ocean Water
179 (VSMOW), covering the isotopic ranges of ambient water vapour at Kathmandu. Each reference
180 standard was measured continuously for a total of 75 min each day at three different humidity
181 levels (25 minutes per level). The dry air passed through Drierite™ desiccant (Merck, Germany)
182 and was delivered to the Picarro analyser for standard measurements. The isotopic composition
183 of atmospheric water vapour is reported as parts per thousand (‰) relative to VSMOW using

$$184 \quad \delta^* = (R_A / R_S - 1) \times 1000 \text{ [‰]}, \quad (1)$$

185
186 where δ^* represents either δD_v or $\delta^{18}\text{O}_v$, and R_A and R_S denote the ratios of heavy to light
187 isotopes ($^{18}\text{O}/^{16}\text{O}$ or D/H) in the sample and standard, respectively (Kendall & Caldwell, 1998;
188 Yoshimura, 2015). As suggested by Dansgaard, (1964), deuterium excess ($\text{d-excess}_v = \delta\text{D}_v - 8 \times \delta^{18}\text{O}_v$)
189 is used as a tracer for moisture source conditions (Liu et al., 2008; Tian et al., 2001). The
190 detailed calibration procedures are outlined in the supplementary material, with the humidity-
191 isotopes response function presented in Figure S2 and all calibration data shown in Figure S3.

192 We examined the hourly isotopic composition of atmospheric water vapour between 7 May and
193 7 June 2021, covering the Tauktae and Yaas cyclones including one week on either side.

194 **2.4 Meteorological data**

195 An automated weather station (AWS, Davis Vantage Pro2) continuously measured air
196 temperature, relative humidity, dew point temperature, wind speed and direction, rainfall
197 amount, surface pressure, etc. at one-minute intervals from 7 May to 7 June 2021.

198 We used the Integrated Multi-satellite Retrievals provided by the Global Precipitation
199 Measurement program (GPM, IMERG dataset) with a spatial resolution of 0.1° for latitude and
200 longitude (Huffman et al., 2017) to analyse the regional rainfall intensity before, during, and
201 after the cyclone events. These high-resolution data allow for the identification of convective
202 rainfall areas and the passage of tropical cyclones (Jackisch et al., 2022). They have been used
203 previously to depict cyclone tracks and associated rainfall intensities (Gaona et al., 2018;
204 Jackisch et al., 2022; Villarini et al., 2011).

205 We further acquired data on outgoing longwave radiation (OLR), zonal and meridional
206 winds, specific humidity, vertical velocity, pressure, vertical distribution of relative humidity and
207 temperature from ERA5 datasets (Hersbach et al., 2020). The data has a spatial resolution of
208 0.25° based on longitude-latitude grids (<https://cds.climate.copernicus.eu/>). OLR data has
209 already been used as an index of tropical convection (Liebmann and Smith, 1996). Additionally,
210 we used cloud-top pressure (CTP) and cloud-top temperature (CTT) data from MERRA-2
211 Reanalysis datasets retrieved from <https://giovanni.gsfc.nasa.gov/>, with a spatial resolution for
212 $0.5^\circ \times 0.625^\circ$, as indicators of convective intensity.

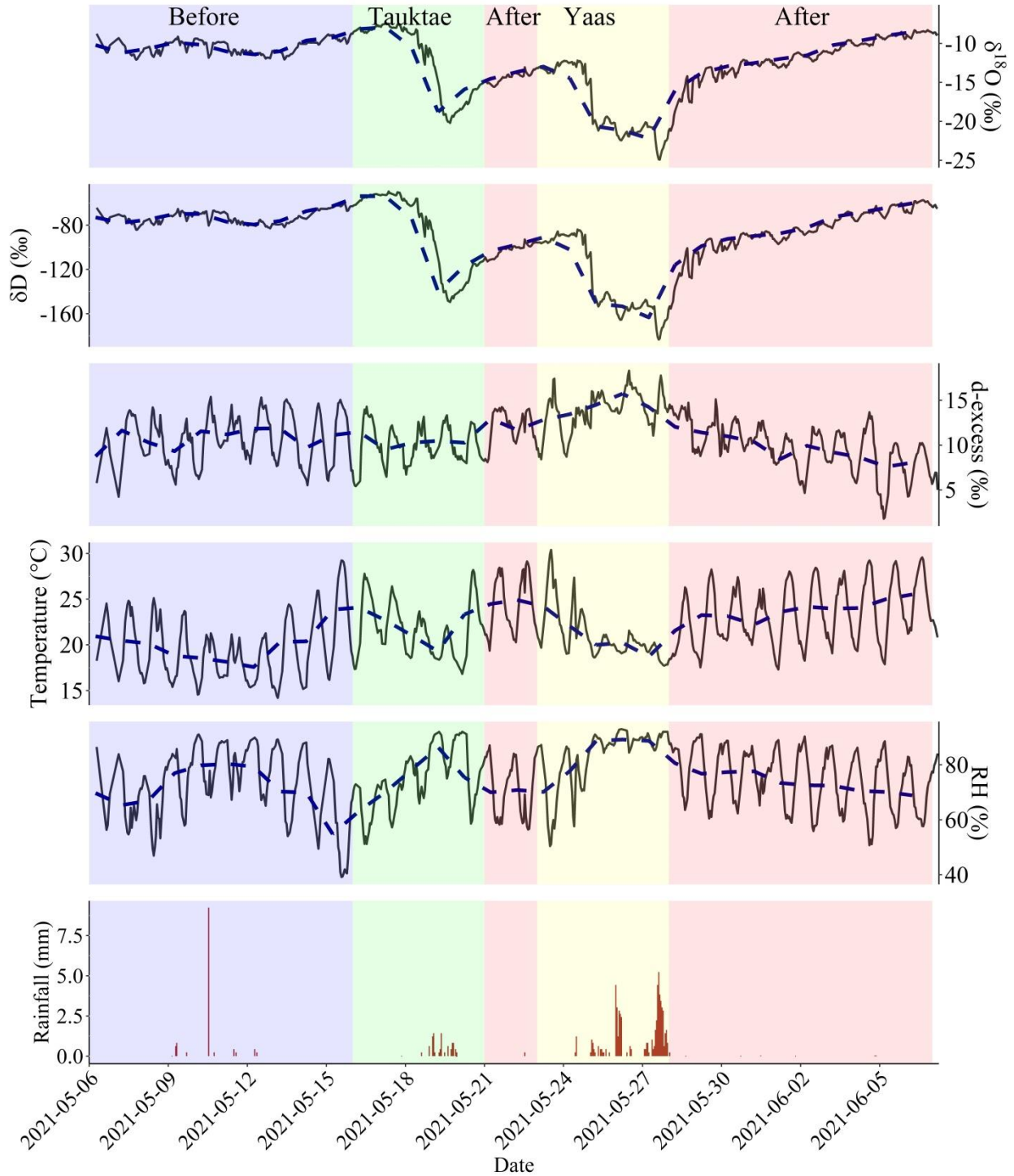
213 **2.5 Moisture backward trajectory analysis**

214 To assess the influence of moisture transport history on the isotopic composition of
215 atmospheric water vapour before, during, and after the cyclone events, we analysed five-day
216 moisture backward trajectories that terminated at the sampling site using the Hybrid Single-
217 Particle Lagrangian Integrated Trajectory (HYSPLIT) model (Draxler and Hess, 1997). The
218 Global Data Assimilation System (GDAS) with a spatial resolution of 1° (Kleist et al., 2009) was
219 used to provide the meteorological forcing for the HYSPLIT model. Variations in specific
220 humidity along the moisture trajectories were also calculated. Considering the variation in
221 boundary layer height at Kathmandu during the study period, ranging from approximately 100 m
222 to 1170 m, and with the majority of the data falling below 600 m, we set the initial starting
223 height for the moisture backward trajectories to 500 m above ground.

224 **3 Results and discussion**

225 **3.1 Isotope dynamics and their relation with local weather before, during,**
226 **and after cyclone events**

227



228

229 **Figure 2 Water vapour isotopic evolution (hourly averages) before, during, and after the**
230 **Tauktae and Yaas cyclone events as indicated by the colour shading along with associated**
231 **surface air temperature, relative humidity (RH), and rainfall amount. The blue dashed line**
232 **represents daily average.**

233 Significant variability was observed in isotopic composition before, during, and after the
234 cyclones at Kathmandu station (Fig. 2 and Table 1). $\delta^{18}\text{O}_v$ and δD_v showed a sudden depletion in
235 isotopic composition at the final stages of both cyclones, coinciding with RH reaching maximum
236 values. The depletion was more pronounced during cyclone Yaas compared to cyclone Tauktae.

237 Before the cyclone Tauktae, $\delta^{18}\text{O}_v$ (δD_v) varied from -7.40 ‰ (-49.53 ‰) to -12.10 ‰ (-
238 84.15 ‰) with an average of -10.04 ‰ (-69.51 ‰) and $d\text{-excess}_v$ ranged from 4.24 ‰ to 15.38
239 ‰ with an average of 10.84 ‰. The isotopic composition clearly shows a downward trend as the
240 remnant of cyclones passed over Kathmandu. $\delta^{18}\text{O}_v$ decreased by over 12 ‰ from 14 May to 20
241 May (Tauktae) and again between 24 May and 29 May (Yaas), reaching minima for $\delta^{18}\text{O}_v$ (δD_v)
242 of -20.21 ‰ (-149.49 ‰) and -24.92 ‰ (-183.34 ‰), respectively. During Tauktae, $\delta^{18}\text{O}_v$ (δD_v)
243 varied from -8.20‰ (-56.06‰) to -20.21‰ (-149.49‰) with an average of -14.73‰ (-106.76‰)
244 and during Yaas the range was from -12.17‰ (-83.85‰) to -24.92‰ (-183.34‰) with an
245 average of -17.87‰ (-129.18‰). Similarly, $d\text{-excess}_v$ during Tauktae varied from 7.97 ‰ to
246 14.24 ‰ with an average of 11.06 ‰ while during Yaas it varied from 8.71 ‰ to 18.29 ‰ with
247 an average of 13.77 ‰. After both cyclones had dissipated, $\delta^{18}\text{O}_v$ (and δD_v) started to recover
248 pre-cyclone values of -8.29 ‰ to -14.94 ‰ (-57.40 ‰ to -109.31 ‰), with an average of -11.09
249 ‰ (-79.38 ‰), and a $d\text{-excess}$ ranged between 1.80 ‰ and 15.11 ‰ with an average of 9.37 ‰.

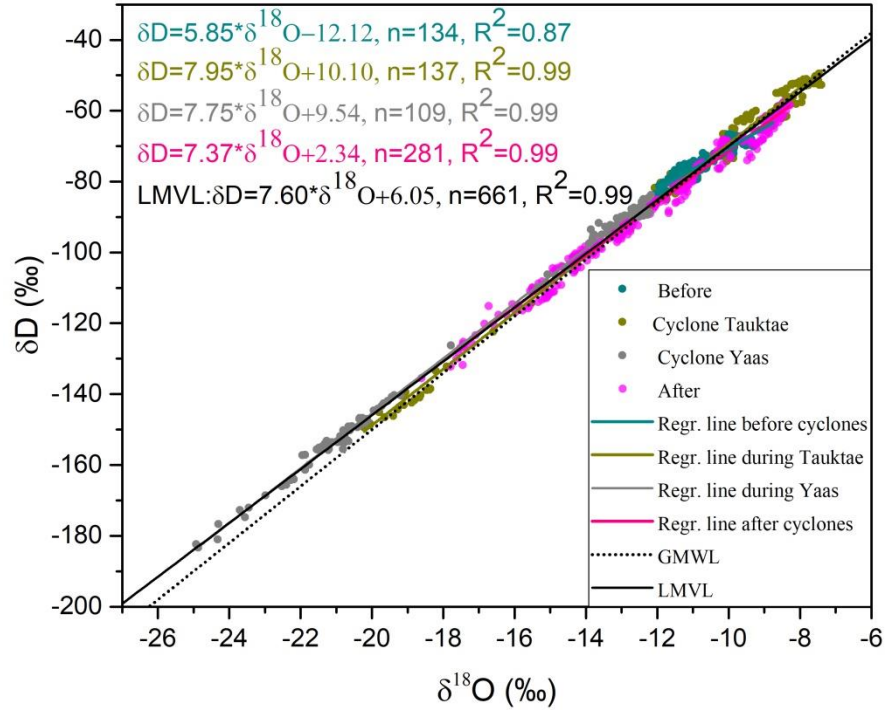
250 The remnants of cyclone Tauktae caused light rain at Kathmandu, with a significant
251 depletion in $\delta^{18}\text{O}_v$ (δD_v) by ~ 8 ‰ (~ 66 ‰) on 20 May compared to the previous day. From the
252 formation of a depression over the AS on 14 May 2021 until the dissipation inland on 19 May ,
253 no significant variation in the isotopic composition in atmospheric water vapour at Kathmandu
254 was observed (Fig. 2). After the dissipation, when the residual Tauktae vapour passed the
255 Kathmandu site producing light rains, $\delta^{18}\text{O}_v$ and δD_v began to decrease independently of the
256 rainfall amount, starting on 19 May around 11:00 h Local Time (LT), from -8.34 ‰ for $\delta^{18}\text{O}_v$
257 and -56.06 ‰ for δD_v and decreasing in one hour to -10.12 ‰ and -68.41 ‰ respectively. This
258 decrease continued for 24 hours reaching a minimum of -20.21 ‰ and -149.49 ‰ for $\delta^{18}\text{O}_v$ and
259 δD_v respectively on 20 May at 12:00 h LT. However, $d\text{-excess}_v$ did not show notable variations
260 during the passage of cyclone Tauktae. $\delta^{18}\text{O}_v$ and δD_v remained depleted from 20 to 22 May.

261 On 24 May, cyclone Yaas formed over the BoB and followed a trajectory through north-
262 eastern India. The effect of cyclone Yaas on $\delta^{18}\text{O}_v$ and δD_v at Kathmandu was observed on 25
263 May with $\delta^{18}\text{O}_v$ (δD_v) dropping rapidly from -12.62 ‰ (-88.71 ‰) on 25 May at 20:00 h LT to -
264 15.07 ‰ (-106.22 ‰) just one hour later. At the same time, $d\text{-excess}_v$ increased from 12.30 ‰ to
265 14.34 ‰. The depletion continued until 28 May with a minimum of $\delta^{18}\text{O}_v$ (δD_v) by -24.92 ‰ (-
266 182.35 ‰) at 16:00 h LT. Yaas had already weakened into a low-pressure area over Bihar in
267 south-eastern Uttar Pradesh, India. $\delta^{18}\text{O}_v$ and δD_v started to increase by about 10 ‰ on 29 May
268 at 16:00 h LT after Yaas had dissipated. From 25 to 29 May, $d\text{-excess}_v$ gradually increased as
269 opposed to $\delta^{18}\text{O}_v$ and δD_v , resulting in a negative correlation with $\delta^{18}\text{O}_v$ and δD_v of -0.60 and -
270 0.55 respectively.

271 The passage of cyclones that had formed over the AS (Tauktae) and BoB (Yaas) caused
272 significant depletion in the isotopic composition and led to cumulative rainfall of 9.2 mm

273 (Tauktae) between 14 May and 20 May 2021 and 59.6 mm (Yaas) between 25 May and 28 May
274 2021 at our site. This depletion is due to cyclone-associated intense rainfall and agrees with
275 previous studies (Krishnamurthy and Shukla, 2007; Rahul et al., 2016). Note the above $\delta^{18}\text{O}_v$
276 minimum (-24.92 ‰) observed during cyclone Yaas is similar to the minima observed in
277 Bangalore, India ($\delta^{18}\text{O}_v = -22.5$ ‰) (Rahul et al., 2016) and Roorkee, India ($\delta^{18}\text{O}_v = -25.35$ ‰)
278 (Saranya et al., 2018) when cyclones evolved over the BoB passed near their sampling sites.
279 These results indicate a similar oceanic source of moisture during cyclones. We discuss the
280 influence of moisture sources in Sect. 3.2.

281 The relation between $\delta^{18}\text{O}_v$ and δD_v varies for the periods before, during, and after the
282 cyclones, showing different slopes and intercepts with the Local Meteoric Vapour Line (LMVL)
283 (Fig. 3). Before the first event, both the slope (5.85) and intercept (-12.12) are significantly lower
284 indicating the strong influence of non-equilibrium processes such as evaporation. During both
285 cyclones the slopes and intercepts resemble those of the Global Meteoric Water Line (GMWL:
286 $\delta\text{D} = 8 \times \delta^{18}\text{O} + 10$) (Fig. 3). After the cyclones, the slope and intercept decreased to 7.37 and 2.34
287 respectively, implying a change of moisture sources and evaporation.



288

289 **Figure 3 Relationships between $\delta^{18}O_v$ and δD_v before, during, and after the cyclone events.**

290 **The regression lines for each period are presented along with GMWL for comparison.**

291 **Table 1 Descriptive statistics of $\delta^{18}O_v$, δD_v , and d-excess_v measured before, during, and**

292 **after the cyclone events.**

Period	$\delta^{18}O_v$ [‰]			δD_v [‰]			d-excess _v [‰]		
	min	max	avg	min	max	avg	min	max	avg
Before	-12.10	-7.40	-10.04	-84.15	-49.53	-69.51	4.24	15.38	10.84
Cyclone Tauktae	-20.21	-8.20	-14.73	-149.49	-56.06	-106.76	7.97	14.24	11.06
Cyclone Yaas	-24.92	-12.17	-17.87	-183.34	-83.85	-129.18	8.71	18.29	13.77
After	-14.94	-8.29	-11.09	-109.31	-57.40	-79.38	1.80	15.11	9.37

293

294 To assess the meteorological influence on the isotopic composition at Kathmandu, we
295 examined the linear correlations between the isotopic composition ($\delta^{18}\text{O}_v$, δD_v , and d-excess_v),
296 and air temperature (T), relative humidity (RH), precipitation amount (P), wind speed (WS), and
297 dew point temperature (T_d) before, during, and after the cyclones (Table 2). Before the cyclones,
298 both $\delta^{18}\text{O}_v$ and δD_v showed a positive correlation with air temperature (i.e., temperature effect)
299 and dew point temperature but no correlations with other meteorological variables (Table 2). The
300 correlation between $\delta^{18}\text{O}_v/\delta\text{D}_v$ and surface air temperature and RH became weaker during the
301 cyclone Tauktae while much stronger ($r=0.60$ for temperature and $r=-0.68$ for RH) during Yaas.
302 During Tauktae, we did not observe any effect of precipitation amount on the isotopic
303 composition, while during Yaas there was a negative correlation ($r=-0.56$). D-excess_v was
304 positively correlated with local air temperature (negatively correlated with local RH) before,
305 during, and after Tauktae, whilst no correlations were observed during Yaas (Table 2).

306

307

308

309

310

311

312

313

314 **Table 2 Linear correlations between the isotopic composition of atmospheric water vapour**
315 **($\delta^{18}\text{O}_v$, δD_v , and d-excess_v) and air temperature (T), relative humidity (RH), precipitation**
316 **amount (P), wind speed (WS), and dew point temperature (T_d) before, during, and after the**
317 **cyclone events. ***, **, and * indicate correlation significance levels of 0.001, 0.01, and 0.05**
318 **respectively.**

Before					
	T	RH	P	WS	T_d
$\delta^{18}\text{O}_v$	0.24 ^{***}	-0.03	-0.41	-0.10	0.51 ^{***}
δD_v	0.44 ^{***}	0.21 ^{**}	-0.37	0.08	0.63 ^{***}
d-excess _v	0.66 ^{***}	-0.64 ^{***}	0.35	0.68 ^{***}	0.28 ^{***}
Cyclone Tauktae					
$\delta^{18}\text{O}_v$	0.15	-0.19	0.11	-0.004	0.07
δD_v	0.21 [*]	-0.25 ^{**}	0.10	0.05	0.11
d-excess _v	0.77 ^{***}	-0.82 ^{***}	-0.22	0.61 ^{***}	0.51 ^{***}
Cyclone Yaas					
$\delta^{18}\text{O}_v$	0.60 ^{***}	-0.68 ^{***}	-0.56 ^{***}	0.02	0.23 ^{**}
δD_v	0.63 ^{***}	-0.70 ^{***}	-0.56 ^{***}	0.05	0.26 ^{**}
d-excess _v	0.10	-0.006	0.19	0.32 ^{**}	0.26 [*]
After					
$\delta^{18}\text{O}_v$	0.17 [*]	-0.19 [*]	-	0.19 [*]	0.09
δD_v	0.30 ^{***}	-0.31 ^{***}	-	0.30 ^{***}	0.20 [*]
d-excess _v	0.62 ^{***}	-0.58 ^{***}	-	0.52 ^{***}	0.55 ^{***}

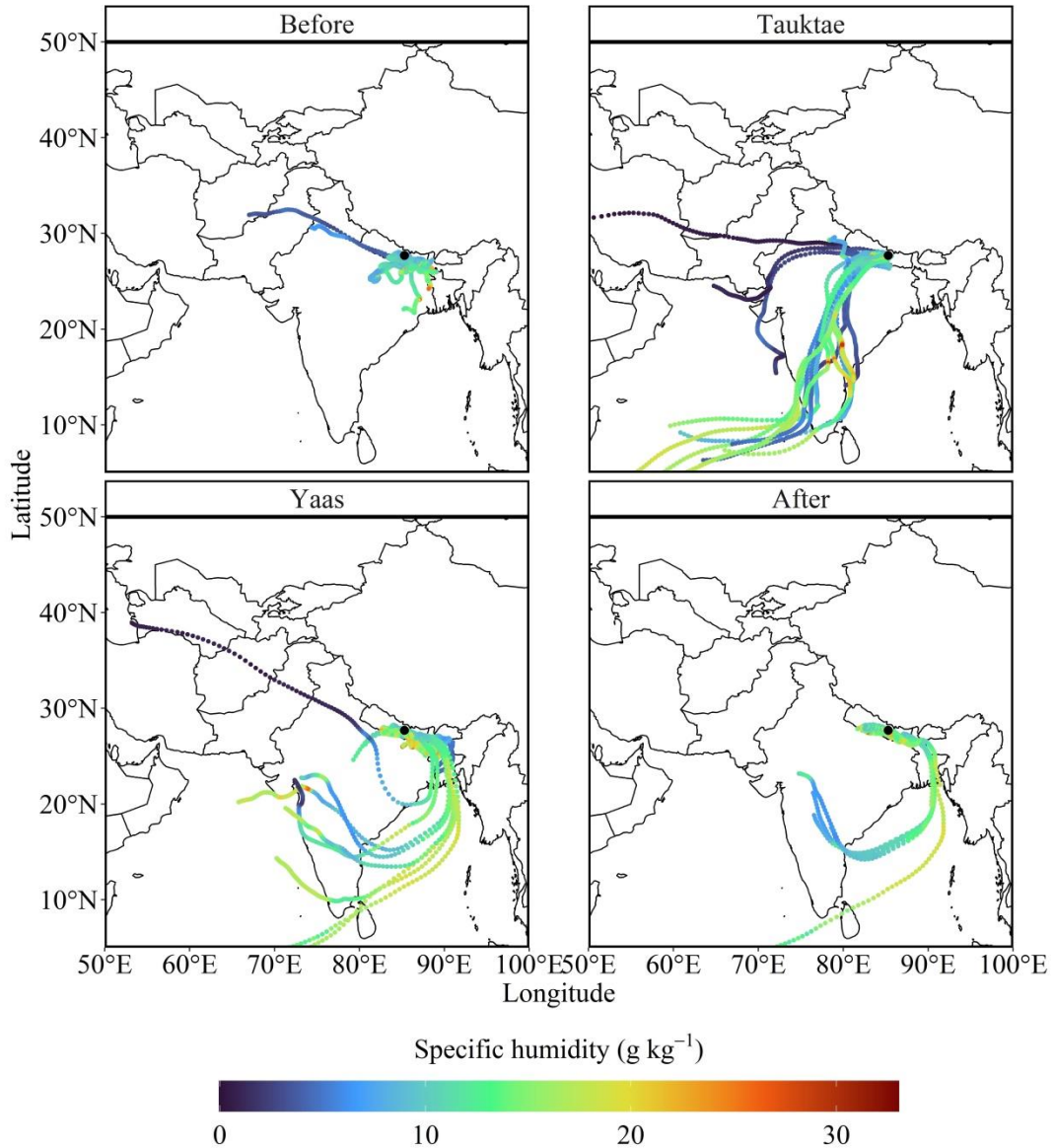
319

320 **3.2 Influence of moisture source**

321 Previous studies suggested that Kathmandu is predominantly impacted by local moisture
322 sources with short and long-range transport of westerlies before the onset of summer monsoon,
323 which is generally dry and characterized by sporadic rainfall with enriched $\delta^{18}\text{O}$ values in
324 precipitation (Adhikari et al., 2020; Chhetri et al., 2014; Yu et al., 2016). We found significant
325 proportions of moisture trajectories prior to cyclone Tauktae either originated locally or by
326 westerlies, characterized by low specific humidity (Fig. 4, upper left panel). These moisture
327 trajectories were traced back to the Gangetic plain before cyclone Tauktae. The associated $\delta^{18}\text{O}_v$

328 and δD_v values for these moisture sources exhibited enrichment, with average values of -10.04‰
329 and -69.51‰ for $\delta^{18}O_v$ and δD_v , respectively. A similar slope (5.85) and intercept (-12.12) of the
330 Local Meteoric Vapour Line before Tauktae to the surface water line calculated in the Gangetic
331 plain (Hassenruck - Gudipati et al., 2023) which provided corroboration for the impact of local
332 evaporation on the isotopic composition.

333 As cyclone Tauktae approached the continent, the primary moisture to Kathmandu was
334 coming from the Arabian Sea, instead of local origins (Fig. 4, upper right panel). The specific
335 humidity along these trajectories exhibited higher levels over the oceans, diminishing as they
336 traversed over land through precipitation (Fig. 4, upper right panel). During this phase, $\delta^{18}O_v$ and
337 δD_v were significantly lower (on average over 4.5‰ and 37‰ for $\delta^{18}O_v$ and δD_v respectively)
338 than measurements preceding the cyclone. Such depletion can be attributed to the progressive
339 rainout along the moisture transport path, wherein heavy isotopes are removed during successive
340 condensation (Xu et al., 2019). Notably, the isotopic composition before the Tauktae-induced
341 rainfall remained enriched, reflecting inflow from the surface layer (Munksgaard et al., 2015).
342 Furthermore, the $d\text{-excess}_v$ variation at Kathmandu during Tauktae may have been influenced by
343 local moisture recycling processes.



344

345 **Figure 4 Five-day backward trajectories reaching the sampling site before, during, and**
 346 **after the cyclone events. Colours denote specific humidity (q in g kg^{-1}) along the**
 347 **trajectories.**

348 During cyclone Yaas, only the BoB vapour contributed to moisture at Kathmandu and
 349 specific humidity along the trajectories over the ocean was high (Fig. 4, bottom left panel). The
 350 high specific humidity over India and surrounding regions during cyclone formation suggest that

351 Yaas lifted a substantial amount of water vapour from the BoB yielding intense rainfall along its
352 path. The isotopic composition during Yaas was more depleted than that of Tauktae with
353 averages of -17.87‰ and -129.18‰ for $\delta^{18}\text{O}_v$ and δD_v respectively. The difference could stem
354 from varied moisture sources, rainout histories, and the respective strengths of each cyclone.
355 Moreover, the high isotopic depletion during cyclone Yaas might be attributed to the disparity of
356 sea surface water $\delta^{18}\text{O}$ between the AS and BoB. The surface water $\delta^{18}\text{O}$ in the BoB is relatively
357 depleted compared to the AS (Lekshmy et al., 2014), which results from a substantial influx of
358 freshwater from rain and runoff originating from the Ganga Brahmaputra river basin
359 (Breitenbach et al., 2010; Singh et al., 2010).

360 Although, the progressive increment was seen in the time series of $\delta^{18}\text{O}_v$ and δD_v after
361 the dissipation of Tauktae (Fig. 2), $\delta^{18}\text{O}_v$ and δD_v in the earlier stage of Yaas were significantly
362 lower compared to Tauktae because there was not enough time for recovery. There was a strong
363 association between $\delta^{18}\text{O}_v$ /or δD_v and local meteorological conditions during cyclone Yaas
364 associated with high relative humidity from the remote ocean (Chen et al., 2021; Xu et al., 2019).
365 Furthermore, the negative correlation of $\delta^{18}\text{O}_v/\delta\text{D}_v$ vs. RH and the fact that $\delta^{18}\text{O}_v/\delta\text{D}_v$ was
366 depleted highlight the influence of humid moisture sources (Yu et al., 2008), which was also
367 confirmed by our moisture backward trajectory analysis (Fig. 4, bottom left panel). A similar
368 correlation was also observed in mid-tropospheric water vapour over the western Pacific
369 associated with intense convective activity (Noone, 2012).

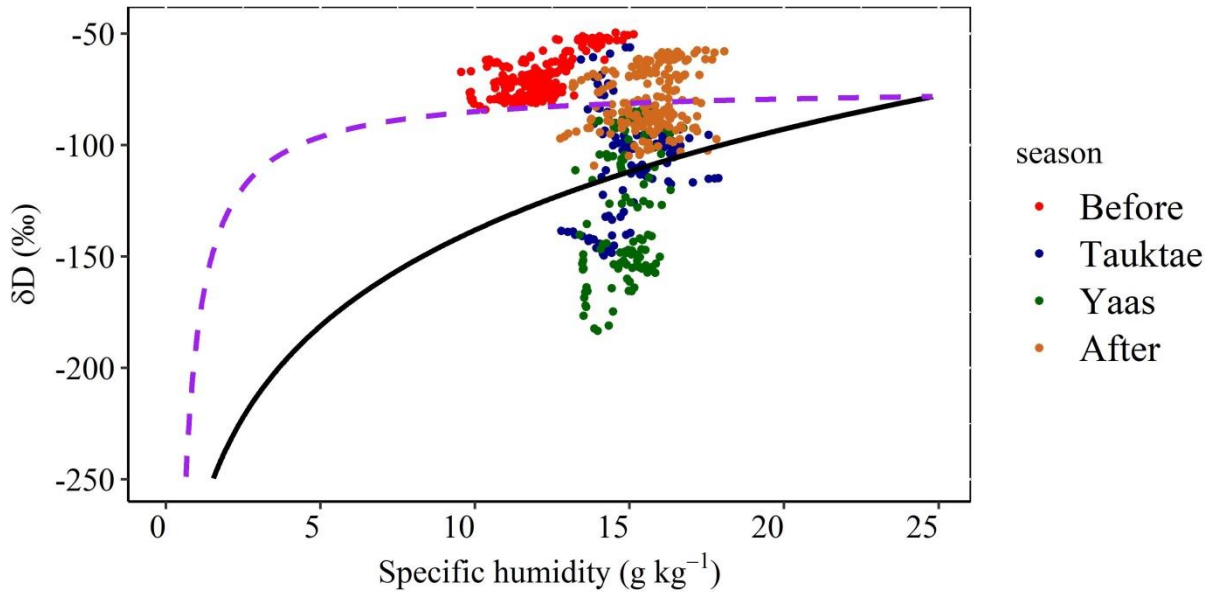
370 In contrast to cyclone Tauktae, the lack of correlation of $d\text{-excess}_v$ with RH and local air
371 temperature during cyclone Yaas implies that local moisture recycling processes are not
372 significant in determining $d\text{-excess}_v$ variation and RH might not be a reliable predictor of kinetic
373 fractionation during evaporation. Previous research conducted in the Indian Ocean (e.g., Midhun

374 et al., 2013; Uemura et al., 2008) suggested that the high relative humidity (i.e. >80%) at the
375 sampling sites weakens the correlation between $d\text{-excess}_v$ and RH. Our observed data also
376 satisfied that condition during Yaas because the majority of isotopic measurements (about 75%)
377 were associated with high relative humidity (>80%), while this fraction was only 25% during
378 Tauktae.

379 Following the dissipation of the cyclones, some portion of moisture at Kathmandu was
380 provided by BoB source together with local evaporation (Fig. 4, bottom right panel). However,
381 the isotopic composition reverted to the original (enriched) levels ($\delta^{18}\text{O}_v = -11.09 \text{ ‰}$, $\delta\text{D}_v = -$
382 79.38 ‰ , and $d\text{-excess}_v = 9.37 \text{ ‰}$). The diminished correlation between $\delta^{18}\text{O}_v/\delta\text{D}_v$ and
383 temperature following the cyclones is attributed to the admixture of vapour originating from
384 plant transpiration during that period (Delattre et al., 2015).

385 We used the vapour $\delta\text{D}_v\text{-}q$ plot combined with the Rayleigh distillation and mixing curve
386 to assess the moisture mixing (Fig. 5). Before the development of cyclone Tauktae and during its
387 early stages, the data points lie well above the mixing curve, indicating that the isotopic
388 variability was mainly dominated by vapour from local evapotranspiration. In contrast, during
389 the latter stage of cyclone Tauktae, δD_v was significantly depleted to levels well below the
390 Rayleigh curve. During the early stage of cyclone Yaas, there are only a few data points between
391 the mixing and Rayleigh curves with the majority well below the Rayleigh curve, particularly
392 during the later stage. During both events, Kathmandu was dominated by deep convection
393 leading to a strong convergence of moisture from both the AS (Tauktae) and the BoB (Yaas).
394 This points towards the influence of convective processes (see Section 3.3) (Galewsky and
395 Samuels-Crow, 2015). After Yaas had dissipated, δD_v gradually increased again with half of the
396 data points clustered between the mixing and Rayleigh curves. The remaining data points were

397 well above the mixing curve, indicating the influence of locally evaporated vapour also
398 evidenced by the moisture back trajectories (Fig. 4, bottom right panel).



399

400 **Figure 5 Scatter plot of hourly averaged δD_v vs. specific humidity (q). The solid black curve**
401 **represents the Rayleigh distillation curve calculated for the initial condition of $\delta D_v = -78.20$**
402 **‰, BoB-averaged δD_v (Lekshmy et al., 2022), SST of 30°C , and RH of 90 %. The dashed**
403 **purple curve represents the mixing line, calculated based on dry continental air ($q = 0.5 \text{ g kg}^{-1}$**
404 **and $\delta D_v = -300 \text{ ‰}$ (Wang et al., 2021)) and the wet source, which corresponds to the**
405 **initial conditions used to calculate the theoretical Rayleigh curve.**

406 3.3 Influence of deep convection associated with cyclones

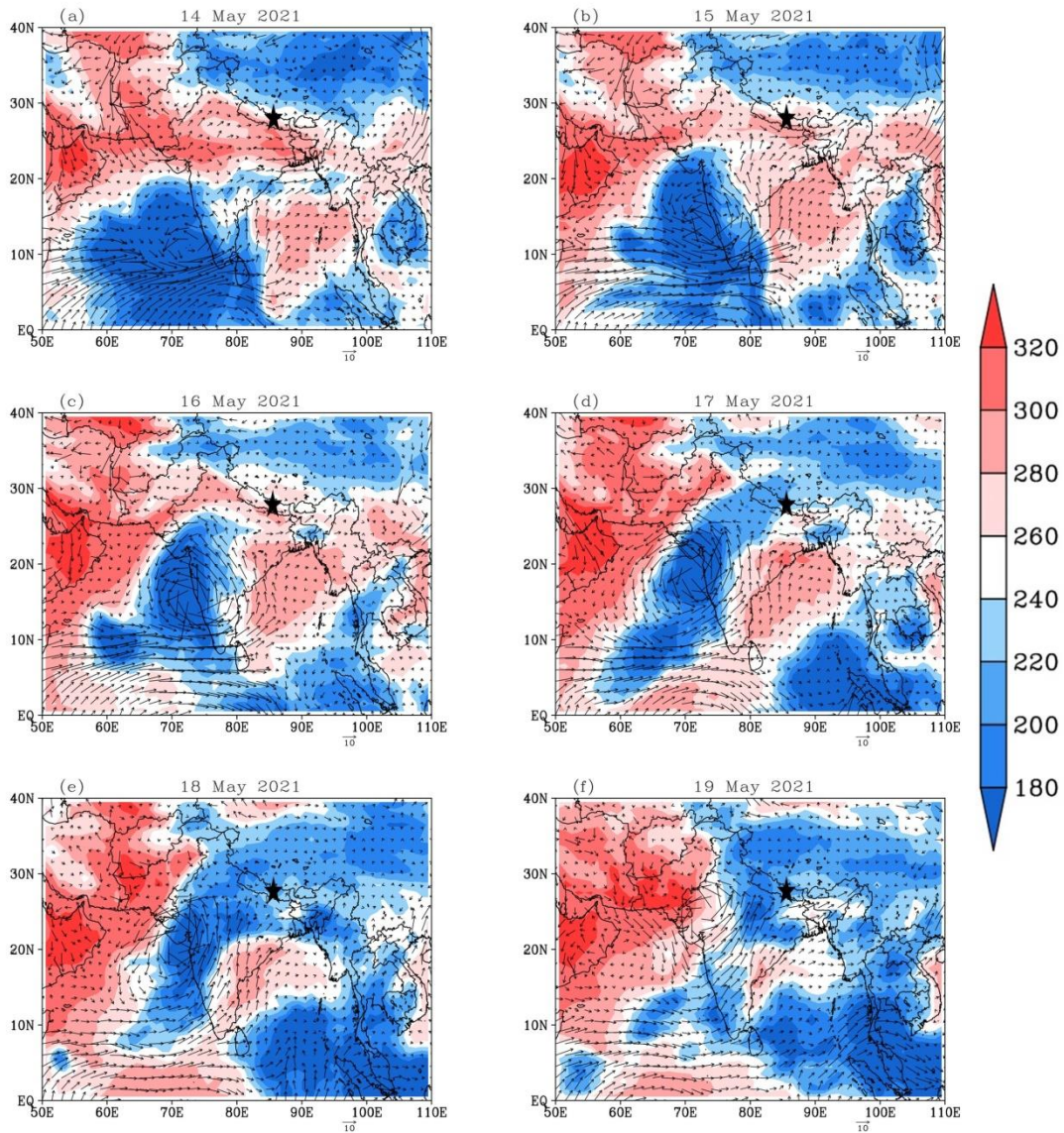
407 One of the likely causes for large isotopic depletion during cyclones might be the
408 associated convective processes. Studies have demonstrated that convective processes within
409 tropical cyclones can cause the depleted isotopic composition of precipitation and atmospheric
410 water vapour (Fudeyasu et al., 2008; Jackisch et al., 2022; Munksgaard et al., 2015) due to a
411 combination of strong cyclonic circulation, intense large-scale convection, heavy precipitation,

412 and high wind speeds (Chen et al., 2021; Xu et al., 2019). We analysed the relationship between
413 the isotopic composition and convective processes, using OLR and vertical velocity as a proxy
414 for convection. Due to the frequent co-occurrence of intense convection and significant mid-
415 tropospheric convergence of moist air, the vertical velocities can also serve as a proxy for
416 convective activity (Lekshmy et al., 2014).

417 Figure 6 and Figure 7 depict the prevalence of strong convective processes associated
418 with both cyclones throughout their lifespan. During the initial days of cyclone formation, OLR
419 exceeded 260 Wm^{-2} in the area of the sampling site and decreased rapidly to below 200 Wm^{-2} in
420 the final stages of both cyclones when approaching the site. Although the amount of precipitation
421 associated with Tauktae (9.2 mm) was much lower than Yaas (59.6 mm), $\delta^{18}\text{O}_v$ depleted by up to
422 12 ‰ during both cyclones. The progressive rainout was evident along the entire cyclone track
423 (Figs. S4 and S5), and the spatial distribution of precipitation was highly correlated with the
424 convective process suggesting rainfall occurred from the deep convective cloud rather than local
425 evaporation. This was confirmed by precipitation variations. The site received its first rainfall on
426 19 May during cyclone Tauktae and on 25 May during cyclone Yaas, as shown in Figure S4 and
427 Figure S5. *In situ* observations confirm that during the days leading up to cyclone Tauktae, the
428 sampling site received a total of 12.2 mm of precipitation with maximum rainfall of 9.2 mm/h
429 recorded on 11 May at 13:00 h LT, equal to the total accumulated rainfall during the entire
430 cyclone. Although the pre and during-Tauktae rainfall amounts are similar, pre-cyclone $\delta^{18}\text{O}_v$
431 and δD_v were significantly more enriched (averages: $\delta^{18}\text{O}_v = -10.04 \text{ ‰}$ and $\delta\text{D}_v = -69.51 \text{ ‰}$)
432 than during Tauktae (averages: $\delta^{18}\text{O}_v = -14.73 \text{ ‰}$ and $\delta\text{D}_v = -106.76 \text{ ‰}$). We compared the
433 values of $\delta^{18}\text{O}_v$, δD_v , and $d\text{-excess}_v$ during both events and also examined them in comparison
434 with the isotopic composition at the beginning of the summer monsoon (June 2021). This initial

435 period of intense and continuous rainfall at our sampling site (Fig. S6) is regulated by the
436 monsoon system originating in the BoB. Consequently, our focus centered on the isotopic
437 distinctions between water vapour on typical rainy days and that associated with cyclone Yaas.

438



439

440 **Figure 6 Regional winds (arrows) and outgoing longwave radiation (colours in Wm^{-2})**

441

during cyclone Tauktae.

442

Following the initiation of the summer monsoon, both $\delta^{18}\text{O}_v$ and δD_v exhibited a

443

progressive depletion, coinciding with a decline in air temperature, an increase in relative

444

humidity (RH), and amplified rainfall amounts (Fig. S6). Despite the daily accumulated rainfall

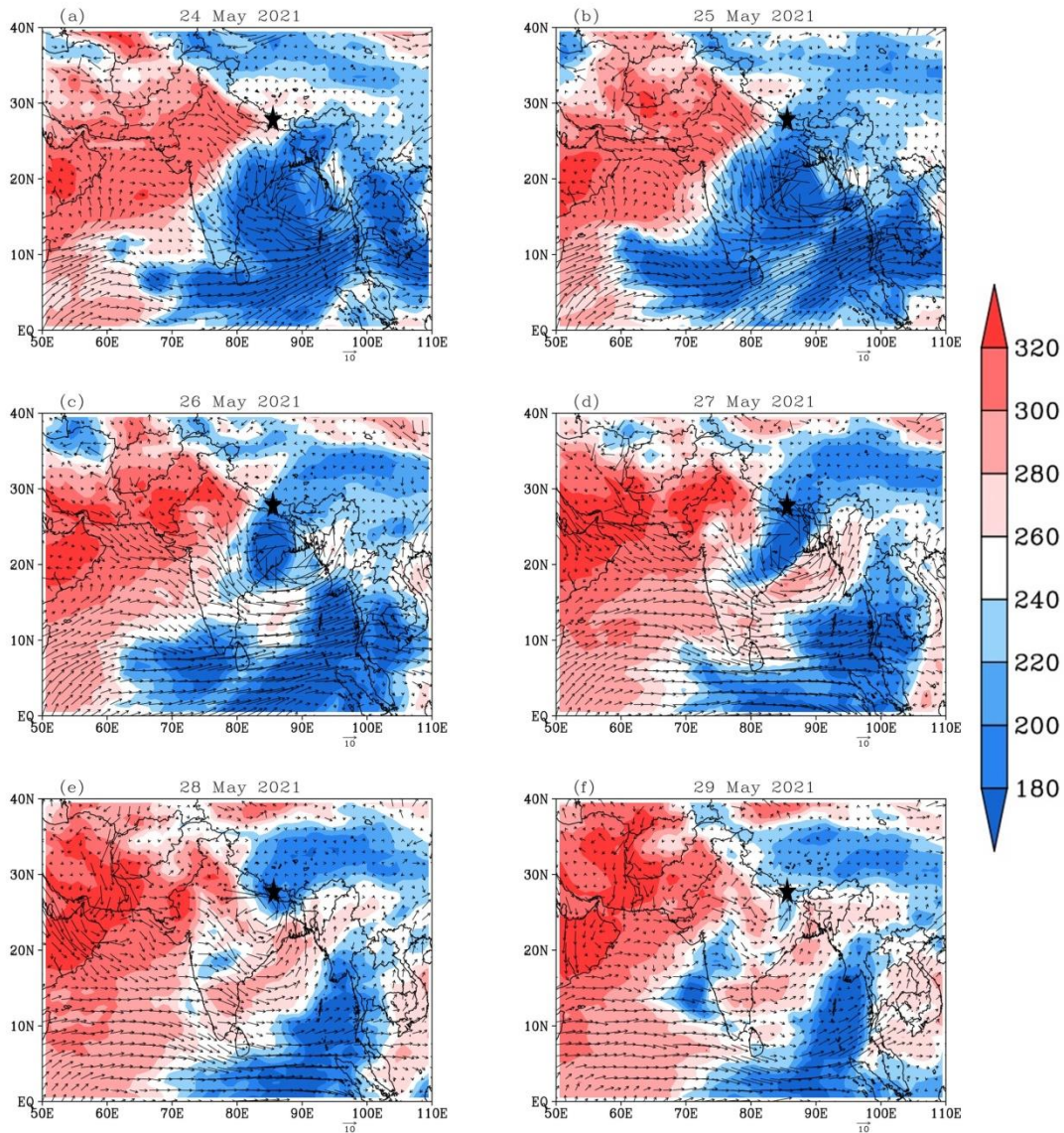
445

and RH being significantly higher during the normal monsoon period, both $\delta^{18}\text{O}_v$ and δD_v were

446

markedly lower during cyclone Yaas (on average by over 2.5‰ and 26‰ for $\delta^{18}\text{O}_v$ and δD_v

447 respectively) compared to typical rainy days. A progressive reduction in $d\text{-excess}_v$ was also
448 evident as the summer monsoon unfolded; a trend typically observed in precipitation d-excess
449 (e.g., Hussain et al., 2015; Acharya et al., 2020; Adhikari et al., 2020) and water vapour d-excess
450 (Tian et al., 2020; Yao et al., 2018; He and Richards, 2016; Wei et al., 2016) in Asian monsoon
451 regions, in contrast to our observations during cyclone Yaas.



452

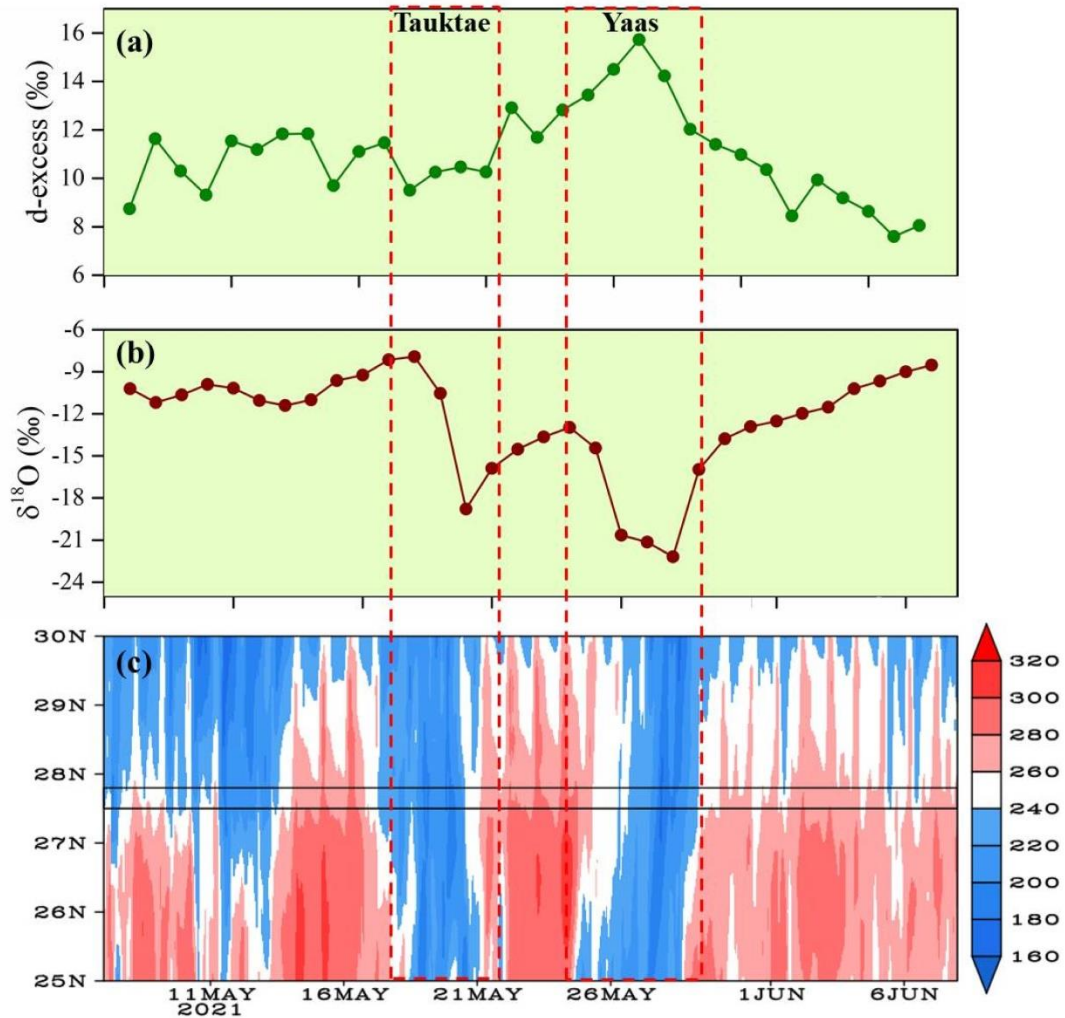
453

Figure 7 Same as Figure 6 but for cyclone Yaas.

454 Given that d-excess has long served as a diagnostic tool for understanding moisture
455 source conditions (Tian et al., 2001; Liu et al., 2008), the distinct behaviour of d-excess_v between
456 cyclone Yaas and the normal monsoon phase suggests that cyclone-related information may be
457 discerned through the isotopic composition recorded at our site. This confirms our previously
458 stated hypothesis that rainfall associated with cyclones causes significantly lower isotope values
459 in vapour due to intense convective systems (Gedzelman et al., 2003; Kurita, 2013), absent in
460 local rain events and days without precipitation (Lekshmy et al., 2022).

461 The influence of convective processes on water vapour isotopic variations at Kathmandu
462 is further supported by the Hovmöller diagram of OLR averaged over 80-90° E, which clearly
463 shows that $\delta^{18}\text{O}_v$ depletion coincides with the presence of clouds (Figs. 8b and c). In contrast, d-
464 excess_v showed dissimilar variations between both cyclones. Before cyclone Tauktae, the daily
465 averaged d-excess_v was above the global average of 10 ‰ (Fig. 8a). Once Tauktae approached
466 our sampling site, d-excess_v decreased from around 12 ‰ to 10 ‰ and continued to oscillate
467 about 10 ‰ until Tauktae had dissipated. As cyclone Yaas approached the measurement site
468 with intense rainfall (Fig. 2), d-excess_v gradually increased while RH increased and air
469 temperature decreased (Fig. 2). Specifically, d-excess_v on 24 May was recorded as 12.82 ‰
470 when surface air temperature and surface RH was about 24 °C and 70 % respectively. On 27
471 May, we noted a 3 ‰ rise in d-excess_v when the surface temperature was reduced by 4 °C and the
472 surface RH was increased by 19 %. The combination of increasing d-excess and decreasing
473 $\delta^{18}\text{O}_v$ highlights the role of vapour recycling due to the subsidence of air masses from stratiform
474 clouds (Kurita et al., 2011). In addition, a large increase in d-excess_v was also recorded in
475 atmospheric vapour during cyclone Ita in 2014 and was attributed to downward moisture
476 transport above the boundary layer (Munksgaard et al., 2015). We did not find any statistically

477 significant correlation during cyclone Yaas between $d\text{-excess}_v$ and RH/Temperature, although
478 RH is considered an important parameter for interpreting $d\text{-excess}$ in atmospheric vapour and
479 precipitation (Pfahl and Sodemann, 2014; Steen-Larsen et al., 2014). The observed co-
480 occurrence of higher $d\text{-excess}_v$, lower temperatures, and high relative humidity (Fig. 2) points to
481 kinetic fractionation processes either at a larger scale or in association with downdrafts (Conroy
482 et al., 2016). Rain re-evaporation under the condition of high saturation deficit is one of the
483 causes of low $\delta^{18}\text{O}_v$ and high $d\text{-excess}_v$. This is due to the addition of re-evaporated vapour
484 during precipitation events, which results in depleted cloud vapour and high $d\text{-excess}_v$ (Conroy et
485 al., 2016; Lekshmy et al., 2014). On normal days high $d\text{-excess}_v$ values were generally
486 accompanied by low RH (Fig. S7) and vice versa. However, the high relative humidity of the
487 surface air together with near saturation conditions vertically (Fig. 9b) during cyclone Yaas, rule
488 out any effect of re-evaporation on increased $d\text{-excess}_v$ values. Such high $d\text{-excess}_v$ values may
489 be associated with downdrafts during convective rain events, transporting isotopically depleted
490 vapour with higher $d\text{-excess}_v$ values from the boundary layer to the surface (Kurita, 2013;
491 Midhun et al., 2013).



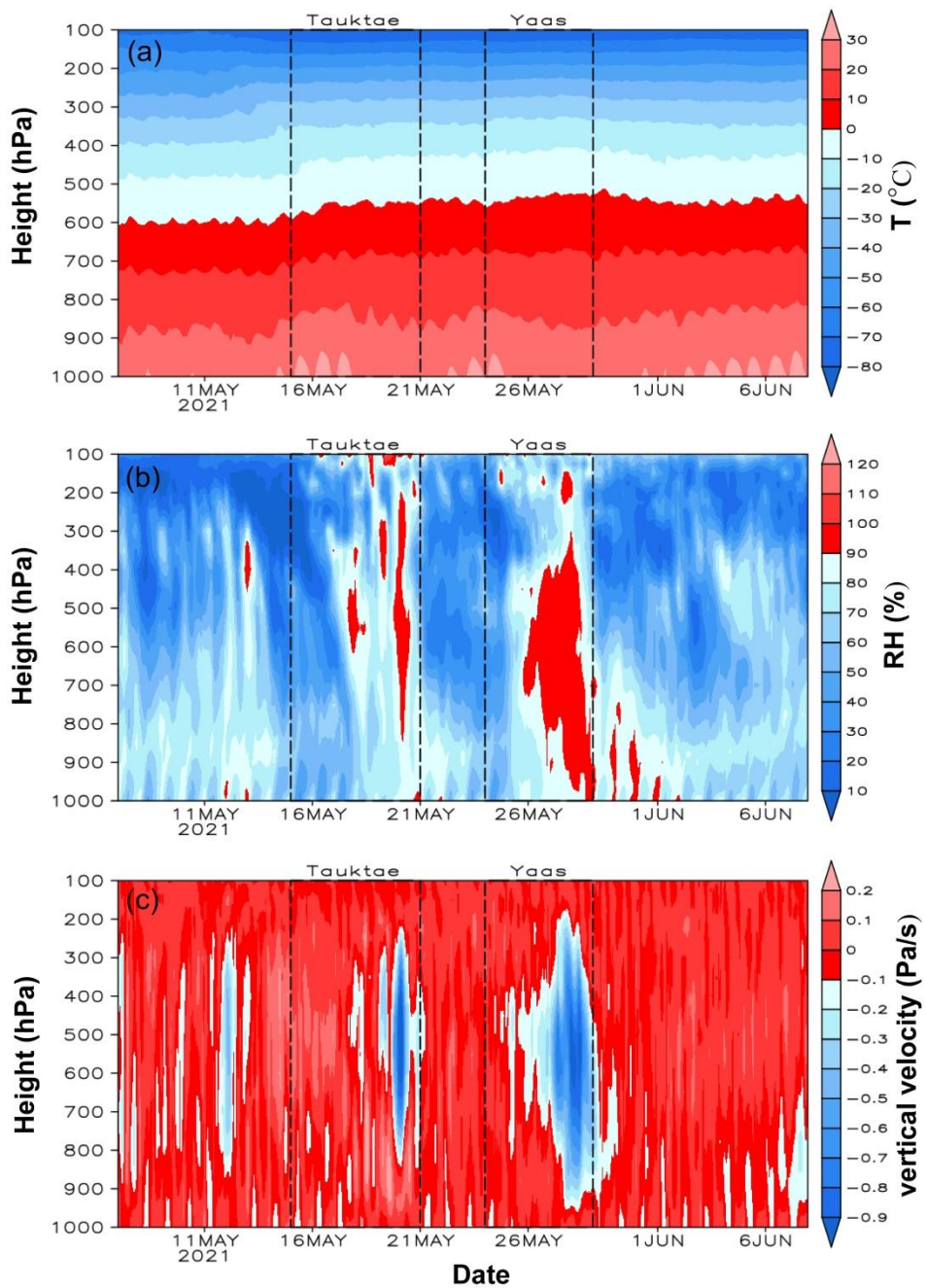
492

493 **Figure 8** Time series of daily averaged $d\text{-excess}_v$ (a), $\delta^{18}\text{O}_v$ (b), and Hovmöller diagram of
 494 **OLR (Wm^{-2}) averaged over $80^\circ \text{E}-90^\circ \text{E}$ (c) The solid parallel lines in (c) depict the latitude**
 495 **range of sampling site.**

496 To clarify the impact of convection on the isotopic composition, we analysed the
 497 distribution of vertical velocity, relative humidity, and air temperature averaged over a box
 498 between $25^\circ\text{N}-28^\circ\text{N}$ and $83^\circ\text{E}-87^\circ\text{E}$ with our measurement site near its center (Fig. 9). Our
 499 results show that strong shifts in $\delta^{18}\text{O}_v$, δD_v , and $d\text{-excess}_v$ during the cyclones were strongly
 500 associated with vertical air motions (Fig. 9c). We observed a general downward movement of air

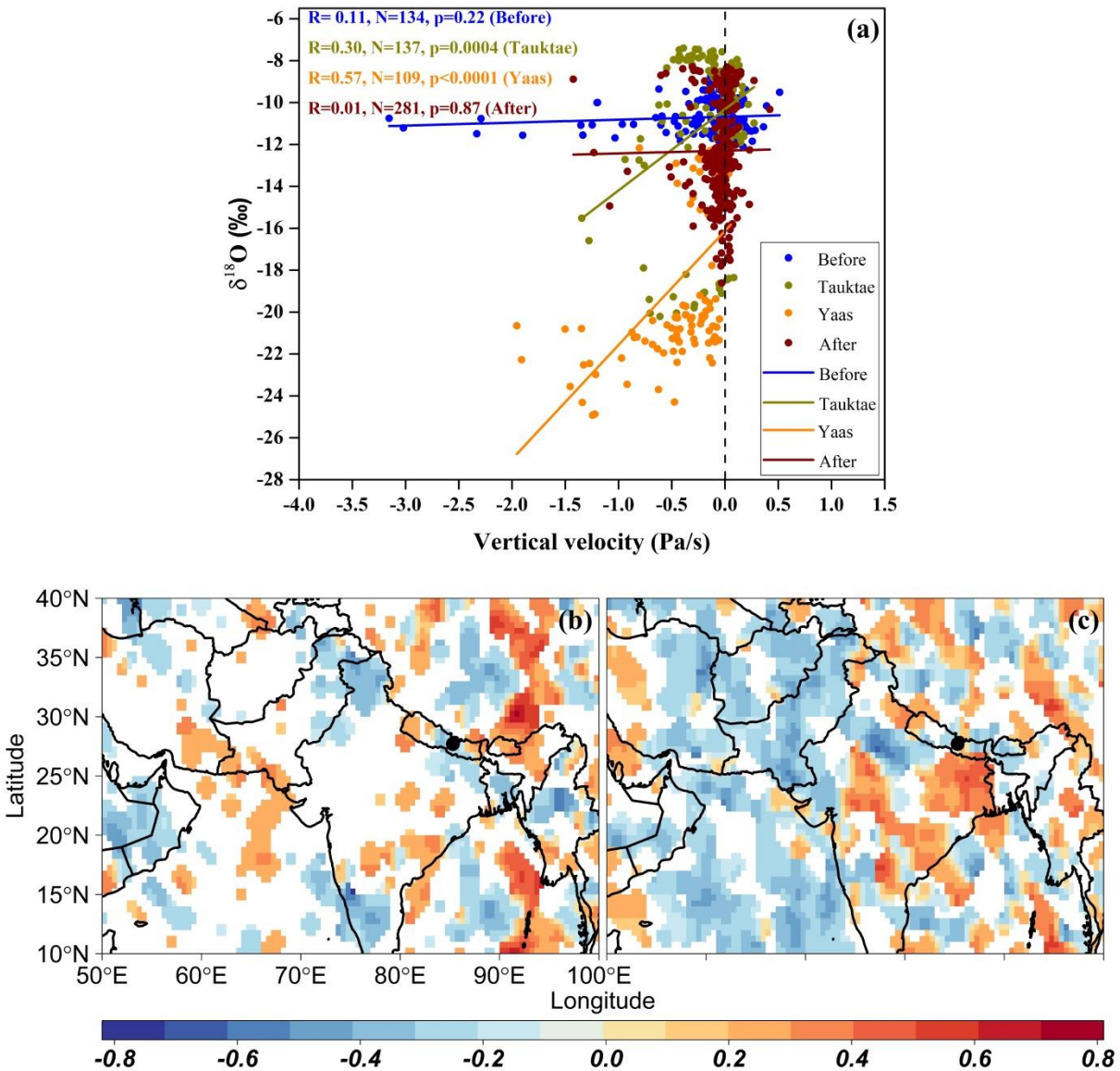
501 before the rain started with Tauktae. The high depletion of $\delta^{18}\text{O}_v$ and δD_v during the final stages
502 of Tauktae (Fig. 2) was accompanied by strong upward air movement extending from 800 hPa to
503 about 200 hPa (Fig. 9c). This upward motion was even stronger during cyclone Yaas and became
504 evident near the measurement site once Yaas made landfall on 26 May. Interestingly, variations
505 in RH at different pressure levels strongly coincided with changes in vertical velocity while the
506 lower troposphere remained near saturation (RH= ~100 %) during the final stages of both
507 cyclones (Fig. 9b). While the air temperature showed the expected decline with altitude (Fig. 9a),
508 there were no significant temporal variations during the entire period, despite the high variation
509 in RH. The strong convective updraft added additional moisture from the warm ocean below,
510 before passing over our measurement site (Lekshmy et al., 2014). Convective updrafts cause
511 moisture to condense quickly and this high-efficiency condensation of heavy rain can result in
512 more depleted $\delta^{18}\text{O}_v$ and δD_v (Lawrence and Gedzelman, 1996). In addition, we found a strong
513 positive correlation between $\delta^{18}\text{O}_v$ and average vertical velocity ($r=0.57$) during Yaas at pressure
514 levels between 300 hPa and 600 hPa (Fig. 10a) in the area surrounding our site. This correlation
515 was weaker ($r=0.30$) during Tauktae. The distinctive relationship between $\delta^{18}\text{O}_v$ and vertical
516 velocity implies that convective processes play a more significant role during Yaas than Tauktae.
517 This result was further supported by the spatial distribution of correlation coefficient between
518 $\delta^{18}\text{O}_v$ and vertical velocity (Fig. 10b, c). During cyclone Tauktae, a significant negative
519 correlation was observed between $\delta^{18}\text{O}_v$ and vertical velocity around the sampling site, while
520 positive correlation areas were identified in western Nepal, certain parts of central India, and the
521 coastal region of the Bay of Bengal (BoB) (Fig. 10b). A comparison with back trajectories
522 unveiled positive correlation only in specific sections along the moisture transport path,
523 suggesting that convective processes may not be the primary driver of isotopic depletion during

524 cyclone Tauktae. Conversely, a positive correlation was evident in the coastal BoB, extending
525 north toward the sampling site during cyclone Yaas (Fig. 10c). The positive correlation areas
526 were considerably larger compared to Tauktae, and these areas closely aligned with the moisture
527 transport path. Hence, higher depletion in $\delta^{18}\text{O}_v$ and δD_v during Yaas, relative to Tauktae, may
528 be attributed to the stronger convection associated with BoB vapour compared to the AS vapour.
529 The BoB is a convectively active region, and previous studies reported greater depletions in $\delta^{18}\text{O}$
530 and δD in precipitation, irrespective of the season (Breitenbach et al., 2010; Lekshmy et al.,
531 2015; Midhun et al., 2018). Another reason we observed different levels of isotope depletion
532 between both cyclones may be related to differences in their proximity to the sampling site.
533 While Yaas came as close as 330 km to our site, Tauktae was about 1050 km away when it
534 dissipated (Fig. S8). The proximity of Yaas may explain the stronger rainfall during that event
535 which enhanced the isotopic fractionation in turn leading to stronger isotopic depletion (Jackisch
536 et al., 2022). Similar results have been documented for precipitation stable isotopes (e.g.,
537 Fudeyasu et al., 2008; Jackisch et al., 2022; Munksgaard et al., 2015; Xu et al., 2019) and water
538 vapour stable isotopes (e.g., Munksgaard et al., 2015; Rahul et al., 2016; Saranya et al., 2018).
539 Even after both cyclones had dissipated, progressive rainfall continued at our sampling site due
540 to the presence of residual moisture from the cyclones. Once these residual effects had
541 diminished and rainfall intensity weakened, $\delta^{18}\text{O}_v$ and δD_v started to increase again (Fig. 2),
542 likely due to evaporative effects (Munksgaard et al., 2015; Xu et al., 2019; Jackisch et al., 2022).



543

544 **Figure 9 Time series of the vertical distribution of air temperature (a), RH (b), and**
 545 **vertical velocity (c) averaged over 25° N- 28° N and 83° E- 87° E with Kathmandu approximately at**
 546 **the centre. Negative (positive) vertical velocities indicate ascending (descending) winds.**



547

548 **Figure 10 (a) Linear regression between $\delta^{18}\text{O}_v$ and the average vertical velocities at**
 549 **pressure levels between 300 hPa and 600 hPa, averaged over 25° N-28° N and 83° E-87° E**
 550 **which has our measurement site near its centre. (b) Spatial distribution of correlation**
 551 **coefficient between $\delta^{18}\text{O}_v$ and vertical velocity during Tauktae. (c) Same as (b) but during**
 552 **Yaas. The vertical black dashed line in (a) represents the threshold separating ascending**
 553 **(negative values) and descending (positive values) air motions.**

554 **3.4 Influence of rainfall**

555 The backward trajectories reveal the impact of separate air masses during cyclones
556 Tauktae and Yaas, specifically between the AS and BoB. We studied the meteorological
557 conditions along the 5-day moisture back trajectories, focusing on the upstream rainout on
558 observed isotopic depletion. During cyclone Tauktae, both $\delta^{18}\text{O}_v$ and δD_v display a strong
559 negative correlation ($r = -0.80$ and $r = -0.79$ for $\delta^{18}\text{O}_v$ and δD_v , respectively, Fig. S9) with total
560 precipitation along the moisture trajectories (i.e., upstream rainout). Moreover, a negative
561 correlation emerges between $\delta^{18}\text{O}_v/\delta\text{D}_v$ and average relative humidity (RH) along the trajectories
562 ($r = -0.69$ for $\delta^{18}\text{O}_v$ and -0.68 for δD_v), suggesting increased upstream rainout corresponds to
563 lower isotope ratios during cyclone Tauktae.

564 In addition, modelled back trajectories indicate that air masses during cyclone Tauktae
565 had a longer transport time when continuous rainout could have enhanced the isotopic depletion
566 of the residual vapour (Fig. 4, upper right panel). The upstream rainfall control could also
567 account for the delayed return of $\delta^{18}\text{O}_v$ and δD_v to more positive values following dissipation.

568 Similar observations have been documented in other regions; for example, the Chinese
569 Typhoons Haitang, Megi, and Soudelor (Xu et al., 2019), the Central American Hurricanes Irma
570 and Otto (Sánchez-Murillo et al., 2019), and Central Texas Hurricane Harvey (Sun et al., 2022)
571 all demonstrate significant negative correlations between upstream rainout and precipitation
572 $\delta^{18}\text{O}$. This suggests that upstream rainout could serve as a widely applicable control on the
573 spatiotemporal variability in tropical cyclones (Sun et al., 2022).

574 In contrast to cyclone Tauktae, neither the total rainfall nor the relative humidity (RH)
575 along the trajectories appears to exert influence on isotopic variation during cyclone Yaas.
576 Instead, a negative correlation was observed between $\delta^{18}\text{O}_v/\delta\text{D}_v$ and local rainfall amount, air

577 temperature, and RH (Table 2). This suggests that the observed isotopic depletion during cyclone
578 Yaas cannot be adequately explained by upstream rainout processes. We assume that sudden
579 changes in local meteorological conditions are a consequence of synoptic processes during the
580 cyclones. The progressive rainout during the cyclone events followed a temperature decrease
581 (Fig. 2) which would result in the $\delta^{18}\text{O}_v/\delta\text{D}_v$ correlation with temperature (Delattre et al., 2015).
582 The cooling of surface air during rainfall, coupled with the isotopic equilibrium of vapour with
583 raindrops, establishes a positive correlation between $\delta^{18}\text{O}_v/\delta\text{D}_v$ and temperature (Midhun et al.,
584 2013). These conditions were favourable during cyclone Yaas because the sampling site
585 experienced consistent rainfall, along with a noticeable increase in relative humidity and a
586 decrease in temperature. This might be one of the reasons for the weaker correlation of $\delta^{18}\text{O}_v/\delta\text{D}_v$
587 with local meteorological variables during Tauktae.

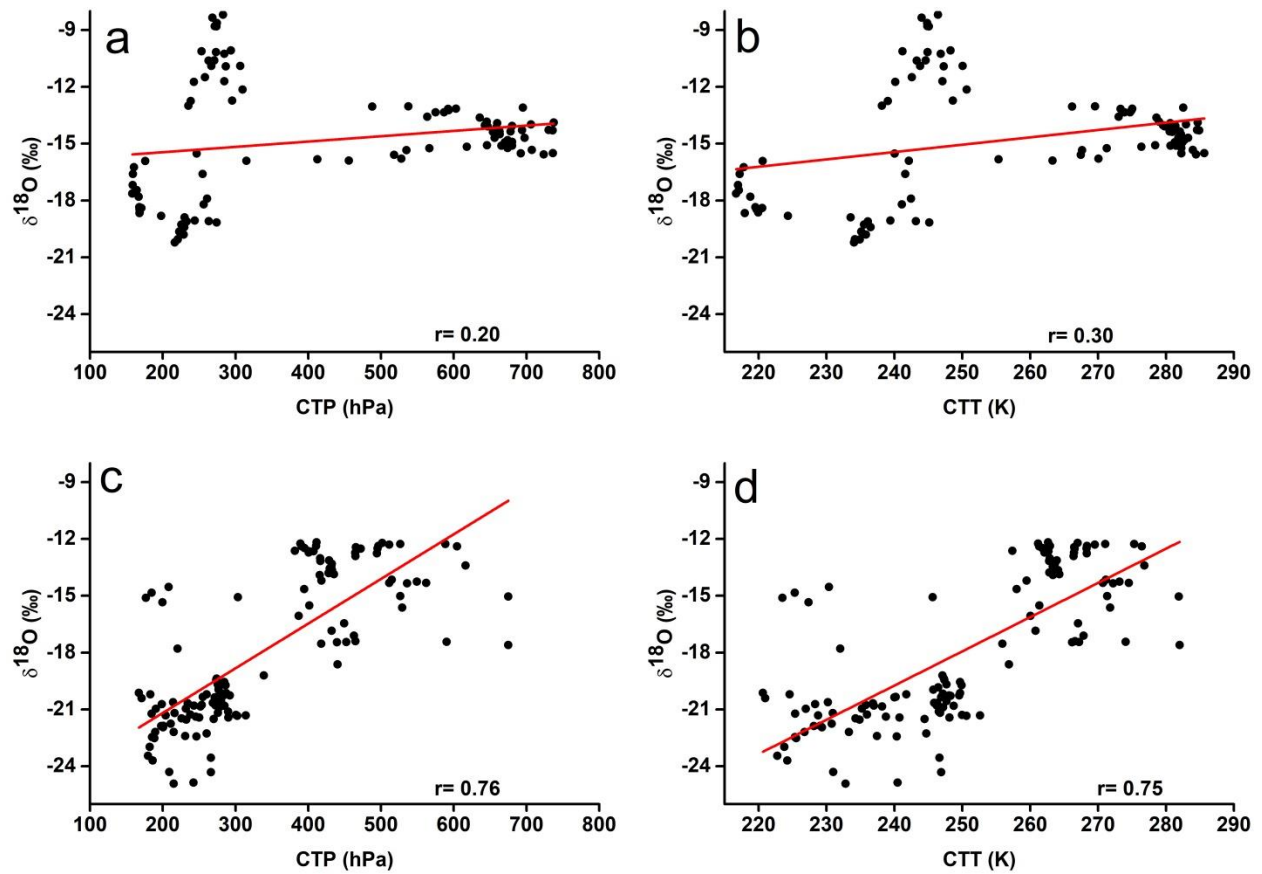
588 Studies have speculated that the impact of precipitation amount is not confined to a
589 strictly local context (Galewsky et al., 2016), but is subject to modulation by convective and
590 large-scale atmospheric properties including downdraft moisture recycling (Risi et al., 2008),
591 large-scale organized convection and associated stratiform rain (Kurita, 2013), as well as
592 regional circulation and shifting moisture sources (Lawrence et al., 2004). Our measurements
593 during cyclone Yaas revealed the presence of an intense convective system over our study site,
594 indicating that the observed effect of rainfall amount may have been governed by moisture
595 convergence (Chakraborty et al., 2016). The subsequent rainfall originating from the convective
596 system, occurring over a region characterized by depleted isotope values, resulted in a negative
597 association between precipitation amount and $\delta^{18}\text{O}_v/\delta\text{D}_v$ (Kurita, 2013). The ^{18}O -depleted water
598 vapour reaching the sub-cloud layer, accompanied by the intense convective downdrafts,

599 subsequently ascended back to the cloud level with the updrafts, in a feedback mechanism
600 proposed by Lekshmy et al., (2014).

601 **3.5 Relation with cloud-top temperature and cloud-top pressure**

602 Given that cloud-top temperature (CTT) and cloud-top pressure (CTP) are reliable
603 indicators of both moisture convergence and convective strength (Cai et al., 2018; Cai and Tian,
604 2016), we investigate the linear correlation between CTT/CTP (averaged over the 27°N-28°N
605 latitude and 85°E-86°E longitude range, with our site located at the center) and $\delta^{18}\text{O}_v$ (Fig. 11).
606 The results demonstrate a weak positive correlation between CTT/CTP and $\delta^{18}\text{O}_v$ during cyclone
607 Tauktae (Fig. 11a, b), and a robust positive correlation during cyclone Yaas (Fig. 11c, d). These
608 correlations exhibit greater strength compared to the correlation observed with local rainfall.
609 Previous research has highlighted positive correlations between $\delta^{18}\text{O}$ and CTT/CTP in the East
610 Asian Monsoon suggesting that intense convection and moisture convergence lead to an increase
611 in cloud-top height and a decrease in CTT, causing a reduction in $\delta^{18}\text{O}$ (Cai and Tian, 2016). The
612 decrease in $\delta^{18}\text{O}_v$ during cyclone Yaas coupled with a decrease in CTT and CTP (i.e. increase in
613 cloud-top height) shows the influence of intensified convective activities and moisture
614 convergence, while the isotopic depletion during cyclone Tauktae is attributed to upstream
615 rainout processes. Furthermore, a negative correlation is evident between $d\text{-excess}_v$ and
616 CTT/CTP, with $r = -0.52$ and $r = -0.60$ during cyclone Yaas. Conversely, a weak positive
617 correlation is observed during cyclone Tauktae, with $r = 0.32$ for both CTT and CTP. This
618 relationship implies that lower CTT and CTP during intense convection relate to increased $d\text{-}$
619 excess_v values during the final stage of cyclone Yaas.

620



621

622 **Figure 11 Relationship between hourly $\delta^{18}\text{O}_v$ and (a) CTT during Tauktae, (b) CTP during**
 623 **Tauktae, (c) CTT during Yaas, and (d) CTP during Yaas.**

624 **4 Conclusion**

625 This study presented the results of continuous measurements of the isotopic composition
 626 of atmospheric water vapour over Kathmandu between 7 May and 7 June 2021 covering two
 627 cyclone events; cyclone Tauktae formed over the Arabian Sea, and cyclone Yaas formed over
 628 the Bay of Bengal. $\delta^{18}\text{O}_v$ (δD_v) during Tauktae varied from -8.20‰ (-56.06‰) to -20.21‰ ($-$
 629 149.49‰) with an average of -14.73‰ (-106.76‰) and during Yaas $\delta^{18}\text{O}_v$ (δD_v) ranges from $-$
 630 12.17‰ (-83.85‰) to -24.92‰ (-183.34‰) with an average of -17.87‰ (-129.18‰). Similarly,
 631 $d\text{-excess}_v$ during Tauktae varied from 7.97‰ to 14.24‰ with an average of 11.06‰ while

632 during Yaas it varied from 8.71 ‰ to 18.29 ‰ with an average of 13.77 ‰. Both cyclones led to
633 significant depletion of $\delta^{18}\text{O}_v$ and δD_v , with $\delta^{18}\text{O}_v$ decreasing by over 12 ‰. We attribute these
634 rapid depletions to changes in moisture sources (local vs. marine) inferred from backward
635 moisture trajectories. The lower intercepts of the Local Meteoric Vapour Line before and after
636 the events highlight the influence of non-equilibrium processes such as evaporation on the
637 isotopic composition. The spatial distribution of OLR, vertical velocity, and regional
638 precipitation during both cyclonic events indicated significant moisture convergence and intense
639 convection at and around the measurement site. This resulted in depleted $\delta^{18}\text{O}_v$ and δD_v , with
640 cyclone Yaas exhibiting stronger moisture convergence and convection, leading to lower $\delta^{18}\text{O}_v$
641 values compared to cyclone Tauktae. This difference may be attributed to robust downdrafts
642 during Yaas-related convective rain events, potentially transporting vapour with higher d-excess_v
643 and lower $\delta^{18}\text{O}_v$ values to the surface. The observed isotopic depletion during cyclone Tauktae
644 can be explained by upstream rainout processes.

645 Overall, our results show that tropical cyclones originating in the BoB and the AS during
646 the pre-monsoon season transport large amounts of isotopically depleted vapour and produce
647 moderate to heavy rainfall over a sizeable region in Nepal. The isotopic composition of
648 atmospheric water vapour and precipitation during the dry season should therefore be interpreted
649 with caution, and the effects of cyclones should not be underestimated. In addition, our results
650 underline the need for simultaneous measurements of the isotopic composition of both
651 atmospheric water vapour and precipitation to better understand post-condensation exchanges
652 between falling raindrops and boundary layer vapour over Kathmandu.

653

654 **Data Availability**

655 The data used in this study will be available in the Zenodo repository.

656 **Competing interests**

657 The contact author has declared that none of the authors has any competing interests.

658 **Acknowledgements**

659 This work was funded by ‘The Second Tibetan Plateau Scientific Expedition and
660 Research (STEP) project’ (Grant No. 2019QZKK0208) and the National Natural Science
661 Foundation of China (Grants 41922002 and 41988101-03). We thank Yulong Yang for his
662 assistance with instrument set-up and initial running.

663 **Author contributions**

664 **Niranjan Adhikari**: Data curation, Formal analysis, Writing - Original draft preparation.
665 **Jing Gao**: Data curation, Conceptualization, Methodology, Supervision, Writing - Review and
666 Editing, Funding acquisition. **Aibin Zhao**: measuring assistance, Writing – Editing. **Tianli Xu**,
667 **Manli Chen**, and **Xiaowei Niu**: measuring assistance. **Tandong Yao**: Supervision, Funding
668 acquisition.

669

670

671

672

673 **5 References**

- 674 Acharya, S., Yang, X., Yao, T., Shrestha, D.: Stable isotopes of precipitation in Nepal Himalaya
675 highlight the topographic influence on moisture transport, *Quat. Int.*, 565, 22–30,
676 <https://doi.org/10.1016/j.quaint.2020.09.052>, 2020.
- 677 Adhikari, N., Gao, J., Yao, T., Yang, Y., Dai, D.: The main controls of the precipitation stable
678 isotopes at Kathmandu, Nepal, *Tellus, Ser. B Chem. Phys. Meteorol.*, 72, 1–17.
679 <https://doi.org/10.1080/16000889.2020.1721967>, 2020
- 680 Bohlinger, P., Sorteberg, A., Sodemann, H.: Synoptic conditions and moisture sources actuating
681 extreme precipitation in Nepal, *J. Geophys. Res. Atmos.*, 122, 12–653,
682 <https://doi.org/10.1002/2017JD027543>, 2017.
- 683 Boschi, R., Lucarini, V.: Water pathways for the Hindu-Kush-Himalaya and an analysis of three
684 flood events, *Atmosphere*, 10, 489, <https://doi.org/10.3390/atmos10090489>, 2019.
- 685 Brand, W.A., Geilmann, H., Crosson, E.R., Rella, C.W.: Cavity ring-down spectroscopy versus
686 high-temperature conversion isotope ratio mass spectrometry; a case study on delta (2) H
687 and delta (18) O of pure water samples and alcohol/water mixtures, *Rapid Commun. mass*
688 *Spectrom*, RCM 23, 1879–1884, <https://doi.org/10.1002/rcm.4083>, 2009.
- 689 Breitenbach, S.F.M., Adkins, J.F., Meyer, H., Marwan, N., Kumar, K.K., Haug, G.H.: Strong
690 influence of water vapor source dynamics on stable isotopes in precipitation observed in
691 Southern Meghalaya, NE India, *Earth Planet. Sci. Lett.*, 292, 212–220,
692 <https://doi.org/10.1016/j.epsl.2010.01.038>, 2010.
- 693 Cai, Z., Tian, L.: Atmospheric controls on seasonal and interannual variations in the

694 precipitation isotope in the East Asian Monsoon region, *J. Clim.*, 29, 1339–1352.
695 <https://doi.org/10.1175/JCLI-D-15-0363.1>, 2016.

696 Cai, Z., Tian, L., Bowen, G.J.: Spatial-seasonal patterns reveal large-scale atmospheric controls
697 on Asian Monsoon precipitation water isotope ratios, *Earth Planet. Sci. Lett.*, 503, 158–169.
698 <https://doi.org/10.1016/j.epsl.2018.09.028>, 2018.

699 Chakraborty, S., Sinha, N., Chattopadhyay, R., Sengupta, S., Mohan, P.M., Datye, A.:
700 Atmospheric controls on the precipitation isotopes over the Andaman Islands, Bay of
701 Bengal, *Sci. Rep.*, 6, 1–11, <https://doi.org/10.1038/srep19555>, 2016.

702 Chan, K.T.F., Chan, J.C.L., Zhang, K., Wu, Y.: Uncertainties in tropical cyclone landfall decay,
703 *npj Clim. Atmos. Sci.*, 5, 93, <https://doi.org/10.1038/s41612-022-00320-z>, 2022.

704 Chen, F., Huang, C., Lao, Q., Zhang, S., Chen, C., Zhou, X., Lu, X., Zhu, Q.: Typhoon Control
705 of Precipitation Dual Isotopes in Southern China and Its Palaeoenvironmental Implications,
706 *J. Geophys. Res. Atmos.*, 126, 1–15, <https://doi.org/10.1029/2020JD034336>, 2021.

707 Chhetri, T.B., Yao, T., Yu, W., Ding, L., Joswiak, D., Tian, L., Devkota, L.P., Qu, D.: Stable
708 isotopic compositions of precipitation events from Kathmandu, southern slope of the
709 Himalayas, *Chinese Sci. Bull.*, 59, 4838–4846, <https://doi.org/10.1007/s11434-014-0547-4>,
710 2014.

711 Conroy, J.L., Noone, D., Cobb, K.M., Moerman, J.W., Konecky, B.L.: Paired stable
712 isotopologues in precipitation and vapor: A case study of the amount effect within western
713 tropical Pacific storms, *J. Geophys. Res. Atmos.*, 121, 3290–3303,
714 <https://doi.org/10.1002/2015JD023844>, 2016.

715 Dansgaard, W.: Stable isotopes in precipitation, *Tellus* 16, 436–468,
716 <https://doi.org/10.3402/tellusa.v16i4.8993>, 1964

717 Delattre, H., Vallet-Coulomb, C., Sonzogni, C.: Deuterium excess in the atmospheric water
718 vapour of a Mediterranean coastal wetland: Regional vs. local signatures, *Atmos. Chem.*
719 *Phys.*, 15, 10167–10181, <https://doi.org/10.5194/acp-15-10167-2015>, 2015

720 Draxler, R.R., Hess, G.D.: Description of the HYSPLIT4 modeling system, 1997.

721 Fudeyasu, H., Ichiyanagi, K., Sugimoto, A., Yoshimura, K., Ueta, A., Yamanaka, M.D., Ozawa,
722 K.: Isotope ratios of precipitation and water vapor observed in Typhoon Shanshan, *J.*
723 *Geophys. Res. Atmos.*, <https://doi.org/10.1029/2007JD009313>, 113, 2008.

724 Galewsky, J., Samuels-Crow, K.: Summertime moisture transport to the southern South
725 American Altiplano: Constraints from in situ measurements of water vapor isotopic
726 composition, *J. Clim.*, 28, 2635–2649, <https://doi.org/10.1175/JCLI-D-14-00511.1>, 2015.

727 Galewsky, J., Steen-larsen, H.C., Field, R.D., Risi, W.C., Schneider, M.: Stable isotopes in
728 atmospheric water vapor and application to the hydrologic cycle., *Rev. Geophys.*
729 submitted, 1–169, <https://doi.org/10.1002/2015RG000512>, 2016.

730 Gaona, M.F.R., Villarini, G., Zhang, W., Vecchi, G.A.: The added value of IMERG in
731 characterizing rainfall in tropical cyclones, *Atmos. Res.*,
732 [doi:10.1016/j.atmosres.2018.03.008](https://doi.org/10.1016/j.atmosres.2018.03.008), 209, 95–102, 2018.

733 Gedzelman, S., Lawrence, J., Gamache, J., Black, M., Hindman, E., Black, R., Dunion, J.,
734 Willoughby, H., Zhang, X.: Probing hurricanes with stable isotopes of rain and water vapor,
735 *Mon. Weather Rev.*, [https://doi.org/10.1175/1520-0493\(2003\)131<1112:phwsio>2.0.co;2](https://doi.org/10.1175/1520-0493(2003)131<1112:phwsio>2.0.co;2),

736 131, 1112–1127, 2003.

737 Han, X., Lang, Y., Wang, T., Liu, C.Q., Li, F., Wang, F., Guo, Q., Li, S., Liu, M., Wang, Y., Xu,
738 A.: Temporal and spatial variations in stable isotopic compositions of precipitation during
739 the typhoon Lekima (2019), China. *Sci. Total Environ.*, 762,
740 <https://doi.org/10.1016/j.scitotenv.2020.143143>, 2021

741 Hassenruck-Gudipati, H.J., Andermann, C., Dee, S., Brunello, C.F., Baidya, K.P., Sachse, D.,
742 Meyer, H., Hovius, N.: Moisture Sources and Pathways Determine Stable Isotope Signature
743 of Himalayan Waters in Nepal, *AGU Adv.*, 4, 1–19, <https://doi.org/10.1029/2022av000735>,
744 2023.

745 He, S., Richards, K.: Stable isotopes in monsoon precipitation and water vapour in Nagqu, Tibet,
746 and their implications for monsoon moisture, *J. Hydrol.*, 540, 615–622,
747 <https://doi.org/10.1016/j.jhydrol.2016.06.046>, 2016.

748 Hersbach, H., Bell, B., Berrisford, P., Hirahara, S., Horányi, A., Muñoz-Sabater, J., Nicolas, J.,
749 Peubey, C., Radu, R., Schepers, D.: The ERA5 global reanalysis, *Q. J. R. Meteorol. Soc.*
750 146, 1999–2049, <https://doi.org/10.1002/qj.3803>, 2020

751 Hoffmann, G., Cuntz, M., Jouzel, J., Werner, M.: A systematic comparison between the
752 IAEA/GNIP isotope network and the ECHAM 4 atmospheric general circulation model,
753 *Isot. Water Cycle Past, Present Futur. a Dev. Sci.*, 303–320, 2005.

754 Huffman, G.J., Bolvin, D., Braithwaite, D., Hsu, K., Joyce, R., Kidd, C., Nelkin, E.J.,
755 Sorooshian, S., Tan, J., Xie, P.: Algorithm Theoretical Basis Document (ATBD) of
756 Integrated Multi-satellite Retrievals for GPM (IMERG), version 4.6. Nasa 29, 2017.

757 Hussain, S., Xianfang, S., Hussain, I., Jianrong, L., Dong Mei, H., Li Hu, Y., Huang, W.:
758 Controlling Factors of the Stable Isotope Composition in the Precipitation of Islamabad,
759 Pakistan, *Adv. Meteorol.*, 2015, 1-11, <https://doi.org/10.1155/2015/817513>, 2015.

760 Jackisch, D., Yeo, B.X., Switzer, A.D., He, S., Cantarero, D.L.M., Siringan, F.P., Goodkin, N.F.:
761 Precipitation stable isotopic signatures of tropical cyclones in Metropolitan Manila,
762 Philippines, show significant negative isotopic excursions, *Nat. Hazards Earth Syst. Sci.*,
763 22, 213–226, <https://doi.org/10.5194/nhess-22-213-2022>, 2022.

764 Joseph, S., Freeland, H.J.: Salinity variability in the Arabian Sea, *Geophys. Res. Lett.*, 32,
765 <https://doi.org/10.1029/2005GL022972>, 2005.

766 Kendall, C., Caldwell, E.A.: Fundamentals of Isotope Geochemistry, *Isot. Tracers Catchment*
767 *Hydrol.*, 51–86, <https://doi.org/10.1016/B978-0-444-81546-0.50009-4>, 1998.

768 Kleist, D.T., Parrish, D.F., Derber, J.C., Treadon, R., Wu, W.-S., Lord, S.: Introduction of the
769 GSI into the NCEP global data assimilation system, *Weather Forecast.*, 24, 1691–1705,
770 <https://doi.org/10.1175/2009waf2222201.1>, 2009.

771 Knapp, K.R., Kruk, M.C., Levinson, D.H., Diamond, H.J., Neumann, C.J.: The international best
772 track archive for climate stewardship (IBTrACS) unifying tropical cyclone data, *Bull. Am.*
773 *Meteorol. Soc.*, 91, 363–376, <https://doi.org/10.1175/2009bams2755.1>, 2010.

774 Krishnamurthy, V., Shukla, J.: Intraseasonal and seasonally persisting patterns of Indian
775 monsoon rainfall, *J. Clim.*, 20, 3–20, <https://doi.org/10.1175/jcli3981.1>, 2007.

776 Kurita, N.: Water isotopic variability in response to mesoscale convective system over the
777 tropical ocean, *J. Geophys. Res. Atmos.*, 118, 10,376-10,390,

778 <https://doi.org/10.1002/jgrd.50754>, 2013.

779 Kurita, N., Noone, D., Risi, C., Schmidt, G.A., Yamada, H., Yoneyama, K.: Intraseasonal
780 isotopic variation associated with the Madden-Julian Oscillation, *J. Geophys. Res. Atmos.*,
781 116, 1–20, <https://doi.org/10.1029/2010JD015209>, 2011.

782 Lawrence, J.R., Gedzelman, S.D., Dexheimer, D., Cho, H.K., Carrie, G.D., Gasparini, R.,
783 Anderson, C.R., Bowman, K.P., Biggerstaff, M.I.: Stable isotopic composition of water
784 vapor in the tropics, *J. Geophys. Res. Atmos.*, 109 (D6),
785 <https://doi.org/10.1029/2003jd004046>, 2004.

786 Lawrence, J.R., Gedzelman, S.D., Gamache, J., Black, M.: Stable isotope ratios: hurricane
787 Olivia, *J. Atmos. Chem.*, 41, 67–82, 2002.

788 Lawrence, J.R., Gedzelman, S.D., Zhang, X., Arnold, R.: Stable isotope ratios of rain and vapor
789 in 1995 hurricanes, *J. Geophys. Res. Atmos.*, 103, 11381–11400,
790 <https://doi.org/10.1029/97jd03627>, 1998.

791 Lawrence, R.J., Gedzelman, D.S.: Low stable isotope ratios of tropical cyclone rains, *Geophys.*
792 *Res. Lett.*, 23, 527–530, <https://doi.org/10.1029/96gl00425>, 1996.

793 Lekshmy, P.R., Midhun, M., Ramesh, R.: Role of moisture transport from Western Pacific
794 region on water vapor isotopes over the Bay of Bengal, *Atmos. Res.*, 265, 105895,
795 <https://doi.org/10.1016/j.atmosres.2021.105895>, 2022.

796 Lekshmy, P.R., Midhun, M., Ramesh, R.: Spatial variation of amount effect over peninsular
797 India and Sri Lanka: Role of seasonality, *Geophys. Res. Lett.*, 42(13), 5500–5507,
798 <https://doi.org/10.1002/2015GL064517>, 2015.

799 Lekshmy, P.R., Midhun, M., Ramesh, R., Jani, R.A.: ^{18}O depletion in monsoon rain relates to
800 large scale organized convection rather than the amount of rainfall, *Sci. Rep.*, 4, 1–5.
801 <https://doi.org/10.1038/srep05661>, 2014.

802 Li, L., Chakraborty, P.: Slower decay of landfalling hurricanes in a warming world, *Nature* 587,
803 230–234, <https://doi.org/10.1038/s41586-020-2867-7>, 2020.

804 Li, Z., Yu, W., Li, T., Murty, V.S.N., Tangang, F.: Bimodal character of cyclone climatology in
805 the Bay of Bengal modulated by monsoon seasonal cycle, *J. Clim.*, 26 (3), 1033–1046,
806 <https://doi.org/10.1175/jcli-d-11-00627.1>, 2013.

807 Liebmann, B., Smith, C.A.: Description of a complete (interpolated) outgoing longwave
808 radiation dataset, *Bull. Am. Meteorol. Soc.*, 77, 1275–1277, 1996.

809 Liu, Z., Tian, L., Yao, T., Yu, W.: Seasonal deuterium excess in Nagqu precipitation: Influence
810 of moisture transport and recycling in the middle of Tibetan Plateau, *Environ. Geol.*, 55,
811 1501–1506, <https://doi.org/10.1007/s00254-007-1100-4>, 2008.

812 Midhun, M., Lekshmy, P.R., Ramesh, R.: Hydrogen and oxygen isotopic compositions of water
813 vapor over the Bay of Bengal during monsoon, *Geophys. Res. Lett.*, 40, 6324–6328,
814 <https://doi.org/10.1002/2013GL058181>, 2013.

815 Midhun, M., Pr, L., Ramesh, R., Yoshimura, K., Kk, S.: The effect of monsoon circulation on the
816 stable isotopic composition of rainfall, *J. Geophys. Res. Atmos.*, 123, 5205–5221,
817 <https://doi.org/10.1029/2017JD027427>, 2018.

818 Mohapatra, M., Srivastava, A.K., Balachandran, S., Geetha, B.: Inter-annual variation and trends
819 in Tropical Cyclones and Monsoon Depressions over the North Indian Ocean. Observed

820 Climate Variability and Change over the Indian Region, Springer Geology, 89–106,
821 https://doi.org/10.1007/978-981-10-2531-0_6, 2016.

822 Munksgaard, N.C., Zwart, C., Kurita, N., Bass, A., Nott, J., Bird, M.I.: Stable isotope anatomy of
823 tropical cyclone Ita, North-Eastern Australia, April 2014, PLoS One 10, 1–15,
824 <https://doi.org/10.1371/journal.pone.0119728>, 2015.

825 Noone, D.: Pairing measurements of the water vapor isotope ratio with humidity to deduce
826 atmospheric moistening and dehydration in the tropical midtroposphere, J. Clim., 25, 4476–
827 4494, <https://doi.org/10.1175/JCLI-D-11-00582.1>, 2012.

828 Pandya, U., Khandelval, S., Sanghvi, H., Joshi, E., Vekaria, G.L., Jaaffrey, S.N.A., Soni, M.:
829 Cyclone ‘TAUKTAE’-Observed through data & satellite images, 2021.

830 Paul, S., Chowdhury, S.: Investigation of the character and impact of tropical cyclone Yaas: a
831 study over coastal districts of West Bengal, India, Saf. Extrem. Environ., 3, 219–235,
832 <https://doi.org/10.1007/s42797-021-00044-y>, 2021.

833 Payne, V.H., Noone, D., Dudhia, A., Piccolo, C., Grainger, R.G.: Global satellite measurements
834 of HDO and implications for understanding the transport of water vapour into the
835 stratosphere, Q. J. R. Meteorol. Soc., 133, 1459–1471, <https://doi.org/10.1002/qj>, 2007.

836 Pfahl, S., Sodemann, H.: What controls deuterium excess in global precipitation? Clim. Past, 10,
837 771–781, <https://doi.org/10.5194/cp-10-771-2014>, 2014..

838 Rahul, P., Ghosh, P., Bhattacharya, S.K., Yoshimura, K.: Controlling factors of rainwater and
839 water vapor isotopes at Bangalore, India: Constraints from observations in 2013 Indian
840 monsoon, J. Geophys. Res., 121, 13,936–13,952, <https://doi.org/10.1002/2016JD025352>,

841 2016.

842 Rajeev, A., Mishra, V.: Observational evidence of increasing compound tropical cyclone-moist
843 heat extremes in India, *Earth's Futur.*, 10, e2022EF002992,
844 <https://doi.org/10.1029/2022ef002992>, 2022.

845 Risi, C., Bony, S., Vimeux, F.: Influence of convective processes on the isotopic composition
846 ($\delta^{18}\text{O}$ and δD) of precipitation and water vapor in the tropics: 2. Physical interpretation of
847 the amount effect, *J. Geophys. Res. Atmos.*, 113, 1–12,
848 <https://doi.org/10.1029/2008JD009943>, 2008.

849 Sánchez-Murillo, R., Durán-Quesada, A.M., Esquivel-Hernández, G., Rojas-Cantillano, D.,
850 Birkel, C., Welsh, K., Sánchez-Llull, M., Alonso-Hernández, C.M., Tetzlaff, D., Soulsby,
851 C., Boll, J., Kurita, N., Cobb, K.M.: Deciphering key processes controlling rainfall isotopic
852 variability during extreme tropical cyclones, *Nat. Commun.*, 10, 1–10,
853 <https://doi.org/10.1038/s41467-019-12062-3>, 2019.

854 Saranya, P., Krishan, G., Rao, M.S., Kumar, S., Kumar, B.: Controls on water vapor isotopes
855 over Roorkee, India: Impact of convective activities and depression systems, *J. Hydrol.*,
856 557, 679–687, <https://doi.org/10.1016/j.jhydrol.2017.12.061>, 2017.

857 Singh, A., Jani, R.A., Ramesh, R.: Spatiotemporal variations of the $\delta^{18}\text{O}$ –salinity relation in the
858 northern Indian Ocean, *Deep Sea Res., Part I* 57 (11), 1422–1431,
859 <https://doi.org/10.1016/j.dsr.2010.08.002>, 2010.

860 Steen-Larsen, H.C., Sveinbjörnsdóttir, A.E., Peters, A.J., Masson-Delmotte, V., Guishard, M.P.,
861 Hsiao, G., Jouzel, J., Noone, D., Warren, J.K., White, J.W.C.: Climatic controls on water

862 vapor deuterium excess in the marine boundary layer of the North Atlantic based on 500
863 days of in situ, continuous measurements, *Atmos. Chem. Phys.*, 14, 7741–7756,
864 <https://doi.org/10.5194/acp-14-7741-2014>, 2014.

865 Sun, C., Tian, L., Shanahan, T.M., Partin, J.W., Gao, Y., Piatrunia, N., Banner, J.: Isotopic
866 variability in tropical cyclone precipitation is controlled by Rayleigh distillation and cloud
867 microphysics, *Commun. Earth Environ.*, 3, <https://doi.org/10.1038/s43247-022-00381-1>,
868 2022.

869 Tian, L., Masson-Delmotte, V., Stievenard, M., Yao, T., Jouzel, J.: Tibetan Plateau summer
870 monsoon northward extent revealed by measurements of water stable isotopes, *J. Geophys.*
871 *Res.*, 106, 28081–28088, <https://doi.org/10.1029/2001JD900186>, 2001.

872 Tian, L., Yu, W., Schuster, P.F., Wen, R., Cai, Z., Wang, D., Shao, L., Cui, J., Guo, X.: Control
873 of seasonal water vapor isotope variations at Lhasa, southern Tibetan Plateau, *J. Hydrol.*,
874 580, 124237, <https://doi.org/10.1016/j.jhydrol.2019.124237>, 2020.

875 Tian, L., Yao, T., Numaguti, A., Sun, W.: Stable isotope variations in monsoon precipitation on
876 the Tibetan Plateau, *J. Meteorol. Soc. Japan.*, 79, 959–966,
877 <https://doi.org/10.2151/jmsj.79.959>, 2001.

878 Uemura, R., Matsui, Y., Yoshimura, K., Motoyama, H., Yoshida, N.: Evidence of deuterium
879 excess in water vapor as an indicator of ocean surface conditions, *J. Geophys. Res. Atmos.*,
880 113, <https://doi.org/10.1029/2008jd010209>, 2008.

881 Verma, K., Gupta, A., 2021. *Cyclone Tauktae: Cyclones, Their Impacts and Disasters Risk*
882 *Management*.

883 Villarini, G., Smith, J.A., Baeck, M.L., Marchok, T., Vecchi, G.A.: Characterization of rainfall
884 distribution and flooding associated with US landfalling tropical cyclones: Analyses of
885 Hurricanes Frances, Ivan, and Jeanne (2004), *J. Geophys. Res. Atmos.*, 116, <https://doi.org/10.1029/2011jd016175>, 2011.

887 Wei, Z., Yoshimura, K., Okazaki, A., Ono, K., Kim, W., Yokoi, M., Lai, C.T.: Understanding
888 the variability of water isotopologues in near-surface atmospheric moisture over a humid
889 subtropical rice paddy in Tsukuba, Japan, *J. Hydrol.*, 533, 91–102,
890 <https://doi.org/10.1016/j.jhydrol.2015.11.044>, 2016.

891 Worden, J., Noone, D., Bowman, K.: Importance of rain evaporation and continental convection
892 in the tropical water cycle, *Nature*, 445, 528–532, <https://doi.org/10.1038/nature05508>,
893 2007.

894 Xu, T., Sun, X., Hong, H., Wang, X., Cui, M., Lei, G., Gao, L., Liu, J., Lone, M.A., Jiang, X.:
895 Stable isotope ratios of typhoon rains in Fuzhou, Southeast China, during 2013–2017, *J.*
896 *Hydrol.*, 570, 445–453, <https://doi.org/10.1016/j.jhydrol.2019.01.017>, 2019.

897 Yoshimura, K.: Stable Water Isotopes in Climatology, Meteorology, and Hydrology: A Review,
898 *J. Meteorol. Soc. Japan*, 93, 513–533, <https://doi.org/10.2151/jmsj.2015-036>, 2015.

899 Yu, W., Yao, T., Tian, L., Ma, Y., Ichiyanagi, K., Wang, Y., Sun, W.: Relationships
900 between $\delta^{18}\text{O}$ in precipitation and air temperature and moisture origin on a south-north
901 transect of the Tibetan Plateau, *Atmos. Res.*, 87, 158–169,
902 <https://doi.org/10.1016/j.atmosres.2007.08.004>, 2008.

903 Yu W, Yao T, Tian L, Ma Y, Wen R, Devkota LP, Wang W, Qu D, Chhetri TB.: Short-term
904 variability in the dates of the Indian monsoon onset and retreat on the southern and northern
905 slopes of the central Himalayas as determined by precipitation stable isotopes, *Clim. Dyn.*,
906 47, 159-72, <https://doi:10.1007/s00382-015-2829-1>, 2016.

907

908

909